Flow simulations in porous media with immersed intersecting fractures

Flow simulations in porous media with immersed intersecting fractures

Stefano Berrone[a,*], Sandra Pieraccini[a], Stefano Scialò[a]

[a]*Dipartimento di Scienze Matematiche, Politecnico di Torino, Corso Duca degli Abruzzi 24, 10129 Torino, Italy.*

Abstract

A novel approach for fully 3D flow simulations in porous media with immersed networks of fractures is presented. The method is based on the discrete fracture and matrix model, in which fractures are represented as two-dimensional objects in a three-dimensional porous matrix. The problem, written in primal formulation on both the fractures and the porous matrix, is solved resorting to the constrained minimization of a properly designed cost functional that expresses the matching conditions at fracture-fracture and fracture-matrix interfaces. The method, originally conceived for intricate fracture networks in impervious rock matrices, is here extended to fractures in a porous permeable rock matrix. The purpose of the optimization approach is to allow for an easy meshing process, independent of the geometrical complexity of the domain, and for a robust and efficient resolution tool, relying on a strong parallelism. The present work is devoted to the presentation of the new method and of its applicability to flow simulations in poro-fractured domains.

Keywords: 3D flows, Darcy flows, matrix-fracture coupled flows, optimization methods for elliptic problems, uncoupled large scale simulations, BEM
2010 MSC: 65N30, 65N50, 68U20, 86-08

1. Introduction

The problem of underground flow simulations is an active research field as a consequence of its relevance in many practical activities, ranging from en-

*Corresponding author
Email addresses: stefano.berrone@polito.it (Stefano Berrone), sandra.pieraccini@polito.it (Sandra Pieraccini), stefano.scialo@polito.it (Stefano Scialò)

vironmental applications, to the geological storage of pollutants, or to energy production purposes, such as oil and gas production or geothermal applications. This work focuses on the simulation of single phase flows in porous media with an embedded network of fractures. Fractures are regions of the rock typically characterized by a dramatic change in the properties of the porous medium, confined in a layer with one of the spatial dimensions, the thickness, that is orders of magnitude smaller than the other two. On the other hand, fracture main dimensions might also span several orders of magnitude, with the simultaneous presence of small fractures and large fractures or faults. Fractures might have a strong impact on the flow, acting as preferential flow paths, or as barriers: the former is the case of highly conductive fractures, with a permeability much greater than that of the surrounding porous medium, the latter being, instead, the case of almost impervious fractures [1, 2]. Only conductive fractures are considered in the present work.

The over-mentioned geometrical complexity and multi-scale nature of the subsurface makes underground flow simulations an extremely challenging task. A major difficulty lies in the representation of the fractures immersed in the porous matrix: due to the very small aperture of fractures with respect to both fracture lengths and domain size, the discretization of the fracture layer would require the introduction of a very large number of elements, thus increasing the computational cost.

The main purpose of the present work is to propose a novel method for underground flow simulations, based on a discrete fracture and matrix model (DFM), capable to tackle these difficulties; the novelty of the approach lies in the reformulation of the problem as a PDE-constrained optimization problem, thus generalizing the method originally proposed by the authors in [3, 4] for discrete fracture networks (DFNs) characterized by an impervious matrix, and further developed in [5, 6, 7, 8, 9, 10, 11].

As an alternative to dual or multi-porosity models [12, 13], or to hybrid-grid models, see [14, 15], DFMs have the advantage of an explicit representation of the fractures, thus improving the accuracy of predictions, mainly when fractures are sparse and with length comparable to that of the simulation domain. DFMs use asymptotic models to describe fractures, in which fractures are seen as two-dimensional objects in the three-dimensional matrix. The Darcy law is used in the three-dimensional domain, whereas an averaged Darcy law across thickness is used in the two-dimensional fractures. Suitable interface conditions are derived and applied in order to close the problem. This approach is usually denoted reduced Darcy model and is followed for example in [16, 2, 17, 18, 19, 20, 21, 22].

The limitation in the use of discrete fracture and matrix models lies in the difficulty of handling the intricate network of fractures immersed in the

porous matrix. In fact, fracture networks for realistic simulations might count up to millions of fractures mutually intersecting with extremely narrow angles. Furthermore, geometrical models of the subsurface are built starting from probabilistic data, thus requiring a large number of simulations corresponding to different realizations of the random variables in order to tackle the issue of uncertainty. Numerical methods requiring some sort of conformity of the computational mesh with the network of fractures might therefore have limited applicability in realistic cases, for the impossibility of generating a mesh given the huge number of geometrical constraints. Different approaches have been recently proposed in order to overcome this limitation. Among others, in [18, 23], the authors use extended finite elements (XFEM) [24] with a mixed formulation for the reduced Darcy problem, allowing fractures to be arbitrarily placed with respect to the mesh of the porous medium. The XFEM with special enrichment functions is used also in [25]. Also the new Virtual Element Method [26, 27, 28, 29, 30, 31] has been successfully used in order to ease the meshing burden for flow simulations in complex networks of fractures [32, 33, 34, 35]. In other works the mesh of the porous medium can not cross fractures, but a non-conformity is allowed between the mesh elements on the fractures and the neighboring elements of the porous medium, as, for example, in [36, 21, 37] where mimetic finite differences (MFD) [38] are used, or in [39] with mixed finite elements. It is also available a vast literature on finite volumes, two point flux approximation (TPFA) or multi-point flux approximation (MPFA) [40], (see e.g. [41, 17, 42, 15, 19, 43, 44, 45]), also recently studied in the general framework of gradient schemes [22].

In this paper we assume fractures to have a higher permeability than the surrounding porous matrix, thus pressure continuity conditions are prescribed across fractures with discontinuities in the velocity; continuity of pressure and flux conservation is also enforced at fracture intersections. Fully embedded fracture networks, i.e., absence of fractures hitting the domain boundary, are allowed, supposing a no-flow condition on the fracture boundaries lying in the interior of the domain. Assuming, as usual, a power law relating the transmissivity of the fractures to their aperture, the no-flow condition at fracture boundaries can be justified by the fact that the aperture of the fractures goes to zero at the fracture boundary.

The reduced Darcy problem is written in primal formulation for both the fractures and the porous matrix. Well posedness is demonstrated, similarly to what proposed in [20]. The optimization approach naturally leads to the decoupling of the original problem into a set of smaller sub-problems. The computational domain is split into smaller sub-domains not crossing the fractures, and, within the optimization framework, only the resolution of

almost independent problems on the small domains is needed. Furthermore, also the problem on the fracture network is decoupled into smaller problems on the single fractures. A properly designed cost functional measures the error in satisfying the prescribed matching conditions at the interfaces of the new sub-problems, and then the global solution is obtained as the constrained minimum of this functional.

The key advantage of this approach, as already shown for the flow problem in DFNs, lies in the possibility of an extremely easy meshing process, that can be performed independently of the interfaces in the domain. Furthermore, the method has an intrinsic scalable nature, with clear advantages for the handling of problems on large domains with intricate fracture networks.

The purpose of the present manuscript is to introduce the formulation of the new approach, demonstrating its equivalence with the "classical" formulation, and the well posedness of the resulting discrete problem. Numerical results are provided in order to show convergence properties of the method and its applicability and effectiveness, providing both quantitative and qualitative comparisons with reference solutions. The realization of numerical tests on realistic configurations is deferred, instead, to a forthcoming work.

The structure of the work is as follows: in Section 2, after an introduction on the relevant notation, a PDE-constrained optimization formulation of the problem is given in the continuous framework. Well posedness of the new formulation is proven. Section 3 reports the discrete formulation of the problem in the optimization framework. A proof of existence and uniqueness of the discrete solution is provided in Section 4. Numerical tests are described in Section 5, whereas some concluding remarks are proposed in Section 6.

2. Problem formulation

2.1. Notation

The present Section introduces the notation used in the paper. As a general introduction, the symbol $\mathcal{D}$, possibly with a subscript, is used to denote an open polyhedral subset of $\mathbb{R}^3$. Indexes k denoting rock matrix blocks $\mathcal{D}_k$ are collected in index sets identified by the symbol $\mathcal{K}$. Planar polygons in $\mathbb{R}^3$ are denoted either by Γ, for matrix block boundaries, or by F, for fractures, and subscripts are used. The set collecting all the indexes ℓ of faces Γ_ℓ is denoted by the letter $\mathcal{L}$. Suitable subsets of $\mathcal{L}$ are marked with subscripts and superscripts as summarized in Table 1. Indexes i of polygons F_i are collected in index sets $\mathcal{I}$, also accompanied by a subscript restricting the elements contained in the set. Segments in the three dimensional space are denoted by letter S, for fracture intersections, or by γ, for fracture boundaries, both with subscripts.

Table 1: Notation for index sets $\mathcal{K}$, $\mathcal{L}$

Label	*Description*
$\mathcal{K}$	all block indexes (dimension $n_{\mathcal{D}}$)
$\mathcal{K}_{\Gamma_\ell}$	block indexes y, z with $y \neq z$ such that $\bar{\Gamma}_\ell = \bar{\mathcal{D}}_y \cap \bar{\mathcal{D}}_z$
$\mathcal{K}_{F_i}$	indexes of blocks having one face on F_i
$\mathcal{L}$	all block-face indexes (dimension n_Γ)
$\mathcal{L}_k$	indexes of block $\mathcal{D}_k$
$\mathcal{L}_{\mathcal{D}}$	indexes of faces not belonging to the boundary of $\mathcal{D}$
$\mathcal{L}_{\partial\mathcal{D}}$	indexes of block-faces belonging to the boundary of $\mathcal{D}$
$\mathcal{L}^\star$	indexes of block-faces lying on a fracture
$\mathcal{L}_{F_i}$	indexes of block-faces lying on fracture F_i
$\mathcal{L}_k^\star$	indexes of faces of block $\mathcal{D}_k$ lying on a fracture
$\mathcal{L}^\diamond$	indexes of block-faces not lying on any fracture ($\mathcal{L}^\diamond = \mathcal{L}_{\mathcal{D}} \setminus \mathcal{L}^\star$)
$\mathcal{L}_{S_m}$	indexes of block-faces contiguous to fracture intersection S_m

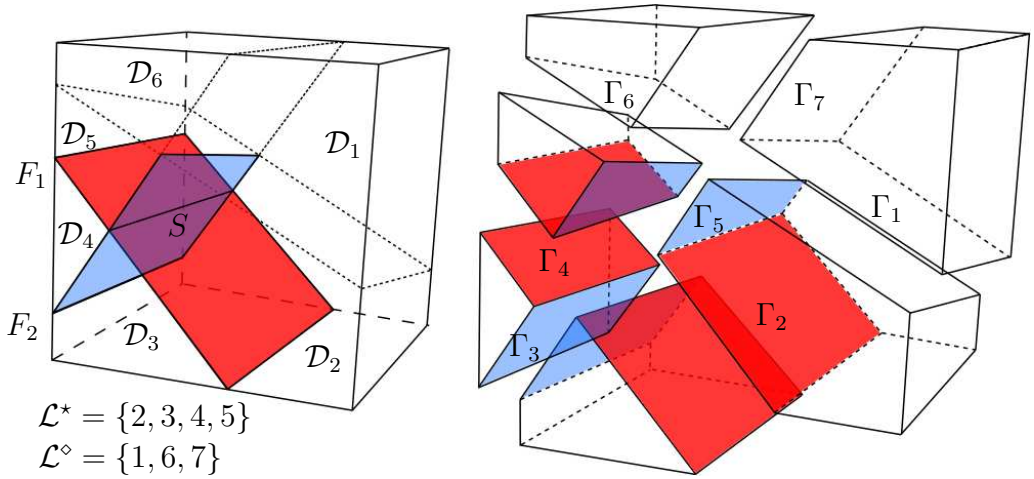

Figure 1: Block splitting and face sets description

Let us consider, in the matrix block $\mathcal{D}$, a set of intersecting planar polygons $\bar{F}_i$, $i = 1, \ldots, I$, representing a discrete fracture network, called Ω and given by the union of the fractures $\bar{F}_i$.

Traces
We assume that the fractures in Ω intersect each other in segments, called traces, each denoted by S_m, $m = 1, \ldots, M$. The set of all the traces in Ω is $\mathcal{S}$, $\mathcal{S}_i$ is the set of traces in $\bar{F}_i$ and, under the assumption that each trace is the intersection of exactly two fractures, i.e. $S_m = \bar{F}_i \cap \bar{F}_j$, we also define, for each $m = 1, \ldots, M$, the set $\mathcal{I}_{S_m} = \{i, j\}$.

Fracture planes
Each fracture $\bar{F}_i$ lies on a plane π_i, and, for each edge $\gamma^e_{F_i}$, $e = 1, \ldots, n_{i,\gamma}$, of the boundary of $\bar{F}_i$ that is in the interior of $\mathcal{D}$ we introduce a plane π^e_i orthogonal to π_i and such that $\gamma^e_{F_i} \subset \pi^e_i$. We denote by $\Pi_i = \pi_i \cup \left(\bigcup_{e=1}^{n_{i,\gamma}} \pi^e_i\right)$ the subset of $\mathbb{R}^3$ given by the union of fracture plane π_i and the planes orthogonal to $\bar{F}_i$ and each containing one of the edges $\gamma^e_{F_i}$, $e = 1, \ldots, n_{i,\gamma}$.

Matrix blocks
The domain $\mathcal{D}$ is then split into open sub-domains (polyhedrons) $\mathcal{D}_k \subset \mathcal{D}$, $k = 1, \ldots, n_{\mathcal{D}}$ that do not cross any of the Π_i, $i = 1, \ldots, I$, i.e. such that $\mathcal{D}_k \cap \Pi_i = \emptyset$, $\forall i = 1, \ldots, I$. An example is reported in Figure 1, where two fractures split the block matrix into six sub-domains. It is possible to observe that a plane orthogonal to the F_2 plane is introduced (with dotted lines), passing through the edge of F_2 lying in the interior of the original matrix block.

We finally remark that this process of block splitting is not optimal and is only used for description purposes.

Block faces
The boundary of each block $\mathcal{D}_k$, $k = 1, \ldots, n_{\mathcal{D}}$ is the union of closed planar polygons in the three dimensional space, each denoted by $\bar{\Gamma}_\ell$, $\ell = 1, \ldots, n_\Gamma$. Let $\mathcal{L}$ be the set of all the indexes of faces $\bar{\Gamma}_\ell$, and $\mathcal{L}_k$ the set of face indexes of block $\mathcal{D}_k$, $k = 1, \ldots, n_{\mathcal{D}}$. Each face $\bar{\Gamma}_\ell$ is either a boundary face, i.e. a portion of the boundary of $\mathcal{D}$, $\partial\mathcal{D}$, or an inner face, shared by exactly two matrix blocks: we denote by $\mathcal{L}_{\partial\mathcal{D}} \subset \mathcal{L}$ the set of indexes of boundary faces, and by $\mathcal{L}_{\mathcal{D}} \subset \mathcal{L}$ the set of indexes of inner faces, such that for each $\ell \in \mathcal{L}_{\mathcal{D}}$, $\bar{\Gamma}_\ell = \bar{\mathcal{D}}_y \cap \bar{\mathcal{D}}_z$, and we collect this couple of indexes in the index set $\mathcal{K}_{\Gamma_\ell} = \{y, z\}$. Each fracture $\bar{F}_i$ in Ω can be obtained as the union of some block faces in $\mathcal{L}$, and we denote by $\mathcal{L}_{F_i}$ the set of face indexes such that $\bar{F}_i = \bigcup_{\ell \in \mathcal{L}_{F_i}} \bar{\Gamma}_\ell$. We also define the set of all face indexes that lie on a fracture, $\mathcal{L}^\star = \bigcup_{i=1}^{I} \mathcal{L}_{F_i}$ and, for each matrix block, the set of block faces lying on a fracture $\mathcal{L}^\star_k = \mathcal{L}_k \cap \mathcal{L}^\star$; we then call $\Gamma_{\mathcal{D}_k} = \bigcup_{\ell \in \mathcal{L}^\star_k} \bar{\Gamma}_\ell$ the portion of the

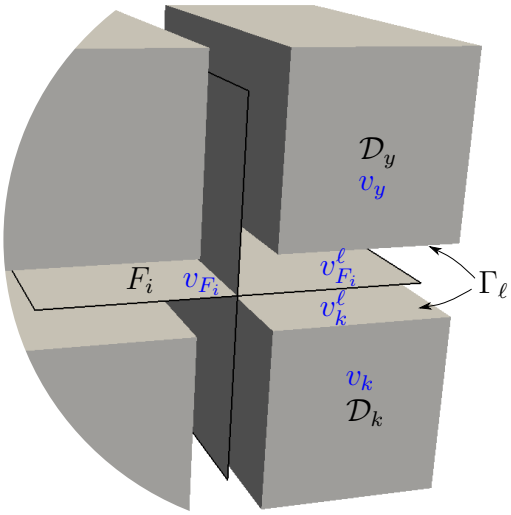

Figure 2: Function notation

boundary of block $\mathcal{D}_k$ that is part of some fracture. We remark that the set $\mathcal{L}_\mathcal{D}$ differs from the set $\mathcal{L}^\star$ since in the former there are also indexes of block faces that are not subsets of fractures of the DFN, and this is a consequence of the strategy chosen to split the original matrix block into sub-blocks not crossing the fractures; we then introduce the function $\varrho : \mathcal{L}^\star \mapsto [1, \ldots, I]$ defined such that, for any $\ell \in \mathcal{L}^\star$, $\bar{\Gamma}_\ell$ is a subset of $\bar{F}_{\varrho(\ell)}$. Finally the set of indexes of faces that are not subset of any fracture is denoted by $\mathcal{L}^\diamond$, i.e. $\mathcal{L}^\diamond = \mathcal{L}_\mathcal{D} \setminus \mathcal{L}^\star$. For each trace S_m in Ω we denote by $\mathcal{L}_{S_m}$ the set of face indexes ℓ such that S_m is part of the boundary of $\bar{\Gamma}_\ell$, i. e. the set of indexes of block faces that are contiguous to fracture intersections: $\mathcal{L}_{S_m} = \left\{\ell \in \mathcal{L} : \partial\bar{\Gamma}_\ell \cap S_m \neq \emptyset\right\}$. With reference to the domain reported in Figure 1, the set $\mathcal{L}^\star$ is given by the face indexes $\mathcal{L}^\star = \{2, 3, 4, 5\}$ whereas $\mathcal{L}^\diamond = \{1, 6, 7\}$. Faces not marked belong to the set $\mathcal{L}_{\partial\mathcal{D}}$. We also have that $\mathcal{L}_{F_1} = \{2, 4\}$, $\mathcal{L}_{F_2} = \{3, 5\}$ and $\mathcal{L}_S = \{2, 3, 4, 5\}$.

By F_i and Γ_ℓ we denote the open subsets of $\mathbb{R}^2$ such that $\bar{F}_i$ and $\bar{\Gamma}_\ell$ are the closure of the image of F_i and Γ_ℓ, respectively, through an affine mapping from $\mathbb{R}^2 \mapsto \mathbb{R}^3$ (see [3] for a possible definition of the mapping).

Function notation

For any sufficiently regular function v defined in $\mathcal{D}$, let us denote by v_k the restriction of v to $\mathcal{D}_k$ and by v^ℓ_k the trace of v_k on Γ_ℓ. Furthermore, by v_{F_i} we indicate the trace of v on F_i and by $v^\ell_{F_i}$ the restriction of v_{F_i} to Γ_ℓ for $\ell \in \mathcal{L}_{F_i}$, see Figure 2.

2.2. Problem setting

We assume, for the sake of simplicity, that homogeneous Dirichlet boundary conditions are prescribed on $\partial\mathcal{D}$ and on the boundaries of the fractures lying on $\partial\mathcal{D}$, which we denote by $\gamma_{F_i,D} = \partial F_i \cap \partial\mathcal{D}$, $\forall i = 1,\dots,I$, whereas homogeneous Neumann boundary conditions are prescribed on the remaining portion of fracture boundary, denoted by $\gamma_{F_i,N} = \partial F_i \setminus \gamma_{F_i,D}$.

Let the transmissivity of the rock matrix be $\mathbf{K}^m$, being $\mathbf{K}^m_k$ its restriction to $\mathcal{D}_k$; let $\mathbf{K}_{F_i}$ be the transmissivity of fracture F_i.

We look for a solution H of the hydraulic head problem in $\mathcal{D}$ that satisfies, for a given load f:

$$
\begin{aligned}
-\nabla\cdot(\mathbf{K}^m_k\nabla H_k) &= f_k && \text{in } \mathcal{D}_k,\ k=1,\dots,n_{\mathcal{D}} && (1)\\
-\nabla_{\pi_i}\cdot\left(\mathbf{K}_{F_i}\nabla_{\pi_i}H^\ell_{F_i}\right) &= \tilde{Q}^\ell && \text{in } \Gamma_\ell,\ \text{for } i=1\dots,I,\ \forall \ell\in\mathcal{L}_{F_i} && (2)\\
H &= 0 && \text{on } \partial\mathcal{D} && (3)
\end{aligned}
$$

being $H^\ell_{F_i}$ the restriction to Γ_ℓ of H_{F_i}, which is, in turn, the trace of H on F_i. In (2), $\tilde{Q}^\ell$ is the unknown load on the face Γ_ℓ. Additional conditions need to be imposed at the block faces Γ_ℓ, imposing continuity of the solution and balance of fluxes. Recalling that $\mathcal{L}_{\mathcal{D}}$ is the set of inner face indexes, $\mathcal{L}^\star$ is the set of indexes of faces that are a subset of a fracture, and that the relative complement $\mathcal{L}^\diamond$ contains indexes of faces that are not contained in any fracture, matching conditions at block faces are written as:

$$
\begin{aligned}
H^\ell_y &= H^\ell_z, && \forall \ell\in\mathcal{L}_{\mathcal{D}},\ y,z\in\mathcal{K}_{\Gamma_\ell}, y\neq z, && (4)\\
\tilde{Q}^\ell_y+\tilde{Q}^\ell_z &= -\tilde{Q}^\ell, && \forall \ell\in\mathcal{L}^\star,\ y,z\in\mathcal{K}_{\Gamma_\ell}, y\neq z, && (5)\\
\tilde{Q}^\ell_y+\tilde{Q}^\ell_z &= 0, && \forall \ell\in\mathcal{L}^\diamond,\ y,z\in\mathcal{K}_{\Gamma_\ell}, y\neq z, && (6)
\end{aligned}
$$

being $\tilde{Q}^\ell_k = (\mathbf{K}^m_k\nabla H_k)\cdot\mathbf{n}^\ell_k$ with $\mathbf{n}^\ell_k$ the unit normal vector to Γ_ℓ oriented outward from $\mathcal{D}_k$.

Additional conditions need to be enforced at fracture intersections, prescribing continuity of the solution and flux continuity at the traces: for $m=1,\dots,M$:

$$
\begin{aligned}
H^\ell_{F_{\varrho(\ell)|S_m}} - H^r_{F_{\varrho(r)|S_m}} &= 0, \quad \text{for } \ell,r\in\mathcal{L}_{S_m},\ \ell\neq r && (7)\\
\sum_{\ell\in\mathcal{L}_{S_m}}\left(\mathbf{K}_{F_{\varrho(\ell)}}\nabla_{\pi_{\varrho(\ell)}}H^\ell_{F_{\varrho(\ell)}}\right)\cdot\mathbf{n}^m_{\Gamma_\ell} &= 0, && (8)
\end{aligned}
$$

being $\mathbf{n}^m_{\Gamma_\ell}$ the unit normal vector to trace S_m with fixed orientation on Γ_ℓ. We remark that continuity of the solution at fracture boundaries is implicitly enforced, thanks to the definition of $H_{F_i} = H_{|F_i}$, $i=1,\dots,I$, and to equation (4).

In the previous matching conditions, equation (4) prescribes the continuity of the solution across the fracture planes, while equation (5) sets the outflow from the matrix blocks as a source term for the equations on the fracture planes. Equations (6), instead, enforce flux balance conditions across block faces that do not lie on any fracture.

2.3. Variational formulation

Let us set the following functional space on the fractures in Ω:

$$\mathrm{H}^1_{i,\gamma}(F_i) = \left\{ v \in \mathrm{H}^1(F_i) : v_{|_{\gamma_{F_i},D}} = 0 \right\};$$

the functional space $\mathrm{H}^1_\Omega(\mathcal{D})$ on the whole domain is defined as:

$$\begin{aligned}\mathrm{H}^1_\Omega(\mathcal{D}) = \big\{ & v \in \mathrm{H}^1_0(\mathcal{D}) : v_{F_i} \in \mathrm{H}^1_{i,\gamma}(F_i),\ i = 1, \dots, I \\ & v_{F_i|S_m} = v_{F_j|S_m},\ m = 1, \dots, M,\ i, j \in \mathcal{I}_{S_m} \Big\}.\end{aligned}$$

The space H^1_Ω can be easily seen to be a Hilbert space endowed with the scalar product $(v, w)_{\mathcal{D},\Omega} = (\nabla v, \nabla w)_{\mathcal{D}} + \sum_{i=1}^{I} (\nabla_{\pi_i} v_{F_i}, \nabla_{\pi_i} w_{F_i})_{F_i}$, $\forall v, w \in \mathrm{H}^1_\Omega$, being ∇_{π_i} the gradient on the tangential plane π_i.

The variational formulation of problem (1)-(8) is given by the following system of equations: find $H \in \mathrm{H}^1_\Omega(\mathcal{D})$ such that, $\forall v \in \mathrm{H}^1_\Omega(\mathcal{D})$

$$(\mathbf{K}^m \nabla H, \nabla v)_{\mathcal{D}} = (f, v)_{\mathcal{D}} + \sum_{i=1}^{I} \sum_{\ell \in \mathcal{L}_{F_i}} \left\langle \tilde{Q}^\ell, v^\ell_{F_i} \right\rangle_{\Gamma_\ell} \tag{9}$$

$$\sum_{i=1}^{I} (\mathbf{K}_{F_i} \nabla_{\pi_i} H_{F_i}, \nabla_{\pi_i} v_{F_i})_{F_i} = -\sum_{i=1}^{I} \sum_{\ell \in \mathcal{L}_{F_i}} \left\langle \tilde{Q}^\ell, v^\ell_{F_i} \right\rangle_{\Gamma_\ell}. \tag{10}$$

The previous problem is well posed as its solution $H \in \mathrm{H}^1_\Omega(\mathcal{D})$ is such that

$$H = \min_{w \in \mathrm{H}^1_\Omega(\mathcal{D})} \mathcal{E}(w),$$

i.e., it corresponds to the unique minimum of the quadratic functional

$$\mathcal{E}(w) = \frac{1}{2} \int_{\mathcal{D}} \left(\left| \sqrt{\mathbf{K}^m} \nabla w \right|^2 - 2 f w \right) + \frac{1}{2} \sum_{i=1}^{I} \int_{F_i} \left| \sqrt{\mathbf{K}_{F_i}} \nabla_{\pi_i} w_{F_i} \right|^2.$$

Another proof of well posedness of the problem in this classical formulation is available for example in [20].

2.4. Optimization formulation

The solution of problem (9)-(10) can be seen as the constrained minimum of a properly designed cost functional. To this end, let us introduce the following functional spaces: $\forall k = 1, \ldots, n_{\mathcal{D}}$,

$$V_k = \mathrm{H}^1_\Omega(\mathcal{D})_{|\mathcal{D}_k} = \left\{ v \in \mathrm{H}^1(\mathcal{D}_k) : v_{|\partial\mathcal{D}\cap\partial\mathcal{D}_k} = 0, \exists w \in \mathrm{H}^1_\Omega(\mathcal{D}) : v = w_{|\mathcal{D}_k} \right\};$$

$V_{F_i} = \mathrm{H}^1_\gamma(F_i)\ \forall i = 1, \ldots, I$; the space $\mathcal{H}^\ell_\Gamma = \mathrm{H}^1(\Gamma_\ell),\ \forall \ell = 1, \ldots, n_\Gamma$ and its dual $\mathcal{Q}^\ell = (\mathcal{H}^\ell_\Gamma)'$; the space $\mathcal{H}^m_S = \mathrm{H}^{\frac{1}{2}}(S_m),\ \forall m = 1, \ldots, M$ and its dual $\mathcal{U}^m = (\mathcal{H}^m_S)'$. Starting from the above definitions, the following product spaces are introduced:

$$V = \prod_{k=1}^{n_{\mathcal{D}}} V_k, \quad V_F = \prod_{i=1}^{I} V_{F_i}, \quad \mathcal{U}_i = \prod_{S_m \in \mathcal{S}_i} \mathcal{U}^m, \quad \mathcal{U} = \prod_{i=1}^{I} \mathcal{U}_i, \quad \mathcal{Q} = \prod_{\ell \in \mathcal{L}_{\mathcal{D}}} \mathcal{Q}^\ell.$$

Let us denote by $U^m_i \in \mathcal{U}^m$ a linear combination of the trace on S_m of a function $H_{F_i} \in V_{F_i}$ and the jump of its co-normal derivative across S_m:

$$U^m_i = \left[\!\left[(\mathbf{K}_{F_i} \nabla_{\pi_i} H_{F_i}) \cdot \mathbf{n}^m_{F_i} \right]\!\right] + \alpha H_{F_i|S_m}, \tag{11}$$

for a given constant $\alpha > 0$, and then we define $U_i = \prod_{S_m \in \mathcal{S}_i} U^m_i \in \mathcal{U}_i$ and $U = \prod_{i=1}^{I} U_i \in \mathcal{U}$. Further, let us define $Q^\ell_k \in \mathcal{Q}^\ell$, for $\ell \in \mathcal{L}_{\mathcal{D}}$ and $k \in \mathcal{K}_{\Gamma_\ell}$ as:

$$Q^\ell_k = \tilde{Q}^\ell_k \cdot \mathbf{n}^\ell_k + \beta H^\ell_k, \tag{12}$$

for a given positive constant β. Then it is $Q^\ell = Q^\ell_k + Q^\ell_y \in \mathcal{Q}^\ell$, $\ell \in \mathcal{L}_{\mathcal{D}}$, $k, y \in \mathcal{K}_{\Gamma_\ell}$, $k \neq y$, and $Q = \prod_{\ell \in \mathcal{L}_{\mathcal{D}}} Q^\ell \in \mathcal{Q}$.

It is now possible to introduce a cost functional J defined for any function $H \in V$, $H_F \in V_F$, $U \in \mathcal{U}$, $Q \in \mathcal{Q}$ as:

$$\begin{aligned} J(H, H_F, U, Q) = \sum_{\ell \in \mathcal{L}^\star} \left\| H^\ell_k - H_{F_{\varrho(\ell)}} \right\|^2_{\mathcal{H}^\ell_\Gamma} + \sum_{\ell \in \mathcal{L}^\diamond} \left\| H^\ell_y - H^\ell_z \right\|^2_{\mathcal{H}^\ell_\Gamma} \\ + \sum_{\ell \in \mathcal{L}^\diamond} \left\| Q^\ell_y + Q^\ell_z - \beta \left(H^\ell_y + H^\ell_z \right) \right\|^2_{\mathcal{Q}^\ell} \\ + \sum_{m=1}^{M} \left(\left\| H_{F_i|S_m} - H_{F_j|S_m} \right\|^2_{\mathcal{H}^m_S} + \left\| U^m_i + U^m_j - \alpha \left(H_{F_i|S_m} + H_{F_j|S_m} \right) \right\|^2_{\mathcal{U}^m} \right), \end{aligned} \tag{13}$$

in which, for each $\ell \in \mathcal{L}_{\mathcal{D}}$, it is $y, z \in \mathcal{K}_{\Gamma_\ell},\ y \neq z$, whereas for each $m = 1, \ldots, M$, $i, j \in \mathcal{I}_{S_m},\ i \neq j$.

The following problems are written in weak formulation on each of the matrix blocks $\mathcal{D}_k$: find $H_k \in V_k$ such that for all $v_k \in V_k$:

$$(\mathbf{K}^m \nabla H_k, \nabla v_k)_{\mathcal{D}_k} + \beta \sum_{\ell \in \mathcal{L}_k} \left(H_k^\ell, v_k^\ell\right)_{\mathcal{D}_k} = (f_k, v_k)_{\mathcal{D}_k} + \sum_{\ell \in \mathcal{L}_k} \left\langle Q_k^\ell, v_k^\ell \right\rangle_{\Gamma_\ell}, \quad (14)$$

and on each of the fracture planes: find $H_{F_i} \in V_{F_i}$ such that for all $v_{F_i} \in V_{F_i}$:

$$(\mathbf{K}_{F_i} \nabla H_{F_i}, \nabla v_{F_i})_{F_i} + \alpha \sum_{S_m \in \mathcal{S}_i} \left(H_{F_i|_{S_m}}, v_{F_i|_{S_m}}\right)_{S_m} = \sum_{\ell \in \mathcal{L}_{F_i}} \left(-(Q^\ell - \beta H^\ell), v_{F_i}\right)_{F_i} + \sum_{S_m \in \mathcal{S}_i} \left\langle U_i^m, v_{F_i} \right\rangle_{S_m}, \quad (15)$$

being $H^\ell = H_y^\ell + H_z^\ell$, with $y, z \in \mathcal{K}_{\Gamma_\ell}$, $y \neq z$. We remark that, if $\alpha, \beta > 0$, problems (14)-(15) are well posed.

The matrix-fracture flow problem, formulated as a PDE-constrained optimization problem, then reads as follows:

$$\begin{aligned} &\min J(H, H_F, U, Q) && (16)\\ &\text{constrained by} && (14)\ \forall k = 1, \ldots, n_{\mathcal{D}} \\ &\text{and by} && (15)\ \forall i = 1, \ldots, I \end{aligned}$$

in which the variables Q and U act as control variables.

Proposition 1. *The solution to* (16) *is equivalent to the solution of equations* (9)-(10).

Proof. It is straightforward to see that the solution of (9)-(10) vanishes the functional and also satisfies the constraints (14)-(15). Conversely, let $(H^*, H_F^*, U^*, Q^*) \in (V, V_F, \mathcal{U}, \mathcal{Q})$ be the solution of (16), and $(H, U, Q) \in (\mathrm{H}^1_\Omega(\mathcal{D}), \mathcal{U}, \mathcal{Q})$ be the solution of (9)-(10). Let us observe that $\mathrm{H}^1_\Omega(\mathcal{D}) \subseteq V$ and $\mathrm{H}^1_\Omega(\mathcal{D})_{|F_i} \subseteq V_{F_i}$, for $i = 1, \ldots, I$. Given $H \in \mathrm{H}^1_\Omega(\mathcal{D})$, let H_F be defined as $H_F = (H_{F_i})_{i=1,\ldots,I}$. Since H, H_F, U, Q satisfy the constraints and $J(H, H_F, U, Q) = 0$, then necessarily $J(H^*, H_F^*, U^*, Q^*) = 0$ and hence $(H^*, H_F^*, U^*, Q^*) \equiv (H, H_F, U, Q)$ for the well posedness of problem (9)-(10). □

Remark 2. *In the above presentation of the problem homogeneous boundary conditions are prescribed on $\partial\mathcal{D}$, for simplicity of notation. The presentation can be readily extended to more general boundary conditions, dividing $\partial\mathcal{D}$ in a Dirichlet part, $\Gamma_D \subseteq \partial\mathcal{D}$, $\Gamma_D \neq \emptyset$, and a Neumann part $\Gamma_N = \partial\mathcal{D} \setminus \Gamma_D$. The functional space of the solution, $\mathrm{H}^1_\Omega(\mathcal{D})$, is re-defined as:*

$$\mathrm{H}^1_\Omega(\mathcal{D}) = \{v \in \mathrm{H}^1(\mathcal{D}) : v = G_\mathrm{D} \text{ on } \Gamma_D,\ v_{F_i} \in \mathrm{H}^1_{i,\gamma}(F_i),\ \forall F_i \in \Omega, \\ v_{F_i|_{S_m}} = v_{F_j|_{S_m}},\ m = 1, \ldots, M,\ i, j \in \mathcal{I}_{S_m}\},$$

where $G_{\mathrm{D}} \in \mathrm{H}^s(\Gamma_D)$ *is the function prescribing the Dirichlet condition on* Γ_D*. A higher regularity than* $s = \frac{1}{2}$ *is required for* G_{D} *in order to ensure meaningful functional spaces for the fractures. A possible choice is* $s = 1$*, which allows for a treatment of boundary conditions in a weak sense, following the approach proposed in [9]. In this case, the functional space on the fractures,* $\mathrm{H}^1_\gamma(F_i)$*, would be defined as:*

$$\mathrm{H}^1_{i,\gamma}(F_i) = \left\{ v \in \mathrm{H}^1(F_i) : v_{|\gamma_{F_i,D}} = f_{\mathrm{D}|\gamma_{F_i,D}} \right\},$$

$f_{\mathrm{D}} \in \mathrm{H}^{\frac{1}{2}}(\gamma_{F_i,D})$.

3. Discrete formulation

The discrete problem is now written in a quite general framework, without referring to a particular discretization choice. The specialization to a particular discretization method (the Boundary Element Method for the matrix blocks and the Finite Element Method for the fracture planes, in the present case) is provided in Appendix A.

Since the method involves quantities on the interfaces, the discretization of the hydraulic head and of fluxes is introduced only on matrix block faces and on the fractures.

3.1. Introduction of DOFs

Let us denote by $\mathbf{x}$ a generic point in the 3D reference system, and let us assume that, on each block face Γ_ℓ, $\ell \in \mathcal{L}$, we have that

$$H^\ell_k = \sum_{j=1}^{N_k^{\Gamma_\ell}} h^\ell_{k,j} \phi^\ell_{k,j}(\mathbf{x}), \qquad Q^\ell_k = \sum_{j=1}^{N_k^{\Gamma_\ell}} q^\ell_{k,j} \phi^\ell_{k,j}(\mathbf{x}), \qquad k \in \mathcal{K}_{\Gamma_\ell},$$

and, for each fracture F_i, $i = 1, \ldots, I$ it is:

$$H_{F_i} = \sum_{j=1}^{N_{F_i}} h_{F_i,j} \varphi_{F_i,j}(\mathbf{x}_{F_i}),$$

being $\mathbf{x}_{F_i}$ a point in the local 2D reference system on F_i. The notation used for the number of basis functions of the discrete variables is summarized in Table 2.

Let us further denote by h^ℓ_k and q^ℓ_k the vectors obtained collecting columnwise all the coefficients $h^\ell_{k,j}$ and $q^\ell_{k,j}$, $j = 1, \ldots, N_k^{\Gamma_\ell}$, respectively, and, similarly, let us denote by h_{F_i} the column vector of coefficients $h_{F_i,j}$, $j =$

Table 2: Notation for the number of degrees of freedom (DOFs)

Label	*Description*
$N_k^{\Gamma_\ell}$	Number of elements of h_k^ℓ and q_k^ℓ, collecting DOFs of H_k^ℓ and Q_k^ℓ on face Γ_ℓ of block $\mathcal{D}_k$
N_k	Number of elements of h_k and q_k, collecting DOFs of H_k^ℓ and Q_k^ℓ on all the faces of block $\mathcal{D}_k$
$N_\mathcal{D}$	Number of elements of $h_\mathcal{D}$ and q, collecting DOFs of H_k^ℓ and Q_k^ℓ on all faces of all blocks
$N_{F_i}^{S_m}$	Number of elements of u_i^m, collecting DOFs of U_i^m on trace S_m of fracture F_i
N^{S_m}	Number of elements of u^m, collecting DOFs of U_i^m and U_j^m on trace S_m of fractures F_i and F_j with $i,j \in \mathcal{I}_{S_m}$ $i \neq j$
$N_{F_i}^{\mathcal{S}_i}$	Number of elements in u_i, collecting DOFs of U_i^m on all the traces of fracture F_i
$N^{\mathcal{S}_i}$	Number of elements in u_i^+, collecting DOFs of both the functions U_x^m for $x \in \mathcal{I}_{S_m}$ on all the traces of F_i, $S_m \in \mathcal{S}_i$
$N^\mathcal{S}$	Number of elements of u, collecting DOFs of all the functions U_i^m on all traces of all fractures
N_{F_i}	Number of elements of h_{F_i}, collecting DOFs of H_{F_i} on fracture F_i
N_F	Number of elements of h_F, collecting DOFs of H_{F_i} on all fractures

$1, \ldots, N_{F_i}$. Starting from the above definitions we build the column vectors $h_k, q_k \in \mathbb{R}^{N_k}$, $k = 1, \ldots, n_\mathcal{D}$ obtained collecting vectors h_k^ℓ and q_k^ℓ, respectively, for increasing values of $\ell \in \mathcal{L}_k$. Finally, vectors $h_\mathcal{D}, q \in \mathbb{R}^{N_\mathcal{D}}$ and $h_F \in \mathbb{R}^{N_F}$ are defined as:

$$h_\mathcal{D} = \begin{bmatrix} h_1 \\ \vdots \\ h_{n_\mathcal{D}} \end{bmatrix}, \qquad q = \begin{bmatrix} q_1 \\ \vdots \\ q_{n_\mathcal{D}} \end{bmatrix}, \qquad h_F = \begin{bmatrix} h_{F_1} \\ \vdots \\ h_{F_I} \end{bmatrix}. \tag{17}$$

Here and in the following the subscript F is used to denote the set of all the fractures in the network.

We also assume that on each trace S_m in Ω it is:

$$U_i^m = \sum_{j=1}^{N_{F_i}^{S_m}} u_{i,j}^m \psi_{F_i,j}^m, \qquad i \in \mathcal{I}_{S_m},$$

and then we introduce vectors $u_i^m \in \mathbb{R}^{N_{F_i}^{S_m}}$ obtained collecting column-wise coefficients $u_{i,j}^m$ for $j = 1, \ldots, N_{F_i}^{S_m}$. We then build vectors $u_i \in \mathbb{R}^{N_{F_i}^{\mathcal{S}_i}}$, obtained grouping column-wise vectors u_i^m for increasing values of index m such that $S_m \in \mathcal{S}_i$, and vectors $u^m \in \mathbb{R}^{N^{S_m}}$, $N^{S_m} = N_{F_i}^{S_m} + N_{F_j}^{S_m}$, obtained collecting vectors u_i^m and u_j^m column-wise for $i,j \in \mathcal{I}_{S_m}$ with $i < j$. Finally,

for $i = 1, \ldots, I$, vectors $u_i^+ \in \mathbb{R}^{N^{\mathcal{S}_i}}$, $N^{\mathcal{S}_i} = \sum_{S_m \in \mathcal{S}_i} N^{S_m}$, are obtained collecting column-wise vectors u^m for increasing values of m such that $S_m \in \mathcal{S}_i$, thus having in u_i^+ coefficients of both the functions U_x^m for $x \in \mathcal{I}_{S_m}$ on all the traces S_m of fracture F_i. Vector $u \in \mathbb{R}^{N^{\mathcal{S}}}$ is then obtained grouping column-wise vectors u^m for increasing values of $m = 1, \ldots, M$.

3.2. Discrete formulation

The discrete functional $J(h, h_F, u, q)$ is obtained replacing the above definitions in the cost functional of equation (13) and substituting the norms in the spaces $\mathcal{H}_\Gamma^\ell$ and $\mathcal{Q}^\ell$ with norms in $\mathrm{L}^2(\Gamma_\ell)$, and the norms in $\mathcal{H}_S^m$ and $\mathcal{U}^m$ with norms in $\mathrm{L}^2(S_m)$. It can be written in compact form as:

$$\begin{aligned} J(h_{\mathcal{D}}, h_F, u, q) &= h_{\mathcal{D}}^T G_{\mathcal{D},\mathcal{D}}^h h_{\mathcal{D}} + (q - 2\beta h_{\mathcal{D}})^T G^q q + 2 h_{\mathcal{D}}^T G_{\mathcal{D},F}^h h_F + \\ & \quad h_F^T \left(G_F^h + 2 G_{F,F}^h \right) h_F + u^T G^u u - 2\alpha h_F^T B_F u. \end{aligned} \tag{18}$$

Also the constraint equations can be written in matrix form, introducing matrices $A_{\mathcal{D}}$, $\mathcal{B}_F^h$ expressing the action of (discrete) operators on the discrete variable $h_{\mathcal{D}}$, matrix A_F on h_F, matrices $\mathcal{B}^q$, $\mathcal{B}_F^q$ on q and $\mathcal{B}^u$ on u. Vectors $b_{\mathcal{D}}$ and b_F collect, instead, source terms and boundary conditions. In particular, concerning the constraint equations on the matrix blocks we formally write:

$$A_{\mathcal{D}} h_{\mathcal{D}} = \mathcal{B}^q q + b_{\mathcal{D}},$$

whereas for equations on the fracture planes:

$$A_F h_F = \mathcal{B}^u u - \mathcal{B}_F^q q + \beta \mathcal{B}_F^h h_{\mathcal{D}} + b_F.$$

The exact expressions of the various terms involved are specified in Appendix A, in the context of a particular discretization choice.

The discrete constrained optimization problem reads as:

$$\min J(h_{\mathcal{D}}, h_F, u, q), \tag{19}$$

$$\text{s.t. :} \quad A_{\mathcal{D}} h_{\mathcal{D}} = \mathcal{B}^q q + b_{\mathcal{D}}, \tag{20}$$

$$A_F h_F = \mathcal{B}^u u - \mathcal{B}_F^q q + \beta \mathcal{B}_F^h h_{\mathcal{D}} + b_F. \tag{21}$$

Let us define $h = [h_{\mathcal{D}}^T, h_F^T]^T$ and $w = [q^T, u^T]^T$, and let us introduce the following matrices:

$$G^h = \begin{bmatrix} G_{\mathcal{D},\mathcal{D}}^h & G_{\mathcal{D},F}^h \\ (G_{\mathcal{D},F}^h)^T & G_F^h + 2G_{F,F}^h \end{bmatrix}, \; G^w = \begin{bmatrix} G^q & 0 \\ 0 & G^u \end{bmatrix}, \; B = \begin{bmatrix} \beta G^q & 0 \\ 0 & \alpha B_F \end{bmatrix},$$

$$\mathcal{B} = \begin{bmatrix} \mathcal{B}^q & 0 \\ \mathcal{B}_F^q & -\mathcal{B}^u \end{bmatrix}, \quad A = \begin{bmatrix} A_{\mathcal{D}} & 0 \\ -\beta \mathcal{B}_F^h & A_F \end{bmatrix}, \tag{22}$$

the optimality conditions for problem (19)-(21) read as:

$$\begin{bmatrix} G^h & -B & A^T \\ -B^T & G^w & \mathcal{B}^T \\ A & \mathcal{B} & 0 \end{bmatrix} \begin{bmatrix} h \\ w \\ \lambda \end{bmatrix} = \begin{bmatrix} 0 \\ 0 \\ \tilde{b} \end{bmatrix} \tag{23}$$

with $\tilde{b} = [b_{\mathcal{D}}^T, b_F^T]^T$.

For further reference, we also set $N_h = N_{\mathcal{D}} + N_F$, $N_w = N_{\mathcal{D}} + N^{\mathcal{S}}$ and $N = N_h + N_w$ and we let $G \in \mathbb{R}^{N \times N}$ and $\mathcal{C} \in \mathbb{R}^{N_h \times N}$ be the matrices defined respectively as follows:

$$G = \begin{bmatrix} G^h & -B \\ -B^T & G^w \end{bmatrix}, \qquad \mathcal{C}^T = \begin{bmatrix} A^T \\ \mathcal{B}^T \end{bmatrix}. \tag{24}$$

4. Well posedness of the discrete problem

In this section we provide a proof of existence and uniqueness of the discrete solution to (19)-(21). The proof is presented here using the BEM for the discretization of the problems on the matrix blocks and finite elements for the discretization of problems on the fractures, following the definitions given in Appendix A. Using similar arguments it is possible to show well posedness of the problem when different discretization choices are used.

First, a technical Lemma is proven, from which it readily follows the main result contained in Theorem 4.

Lemma 3. *Let matrix A, defined as in (22), be full rank, let matrix $\mathcal{C}$ be defined as in (24) and let Z be a matrix obtained collecting row-wise column vectors z_ξ, $\xi = 1, \ldots, N_w$, forming a basis of $\ker(\mathcal{C})$, then matrix $Z^T G Z$ is positive definite.*

Proof. We start observing that matrix A is full rank as both matrices $A_{\mathcal{D}}$ and A_F are full rank under the assumption that $\alpha, \beta > 0$. Then $\dim(\ker(\mathcal{C})) = N_w$, since for any vector $w^* \in \mathbb{R}^{N_w}$ it is possible to find $h^* \in \mathbb{R}^{N_h}$ such that $Ah^* = Bw^*$. To construct a basis of $\ker(\mathcal{C})$, let us take e_ξ, the ξ-th vector of the canonical basis of $\mathbb{R}^{N_w}$, and let us set $z_\xi = (A^{-1}Be_\xi, e_\xi)$. According to the index ξ, e_ξ might correspond to: *i*) a non-null function Q_k^ℓ for some $\ell \in \mathcal{L}^\star$ and $k \in \mathcal{K}_{\Gamma_\ell}$; *ii*) a non-null function Q_k^ℓ for some $\ell \in \mathcal{L}^\diamond$, and $k \in \mathcal{K}_{\Gamma_\ell}$; *iii*) a non-null function U_i^m for some $i = 1, \ldots, I$ and $S_m \in \mathcal{S}_i$. Let us consider the case *i*) and in particular let us assume that $Q_{k^*}^{\ell^*} = \phi_{k^*,j}^{\ell^*}$ for certain indexes j, $\ell^* \in \mathcal{L}^\star$ and $k^* \in \mathcal{K}_{\Gamma_{\ell^*}}$. Let now $H_{F_{\varrho(\ell^*)}}$ be the solution on the fracture on which Γ_{ℓ^*} lies and let $H_{k^{**}}^{\ell^*}$ be the solution on Γ_{ℓ^*} of block $\mathcal{D}_{k^{**}}$, with $k^*, k^{**} \in \mathcal{K}_{\Gamma_{\ell^*}}$, $k^* \neq k^{**}$. Then it is either $\|H_{k^{**}}^{\ell^*} - H_{F_{\varrho(\ell^*)}}\|_{\mathrm{L}^2(\Gamma_{\ell^*})} > 0$ or

$\|H^{\ell^*}_{k^*} - H_{F_{\varrho(\ell^*)}}\|_{\mathrm{L}^2(\Gamma_{\ell^*})} > 0$, and thus, in both cases, $z_\xi^T G z_\xi > 0$. Let us move to case *ii*) and let us now assume that $Q^{\ell^\dagger}_{k^\dagger} = \phi^{\ell^\dagger}_{k^\dagger,j}$ for certain indexes j, $\ell^\dagger \in \mathcal{L}^\diamond$ and $k^\dagger \in \mathcal{K}_{\Gamma_{\ell^\dagger}}$, differing from the previous case for the fact that now $\ell^\dagger$ corresponds to a face not matching with a fracture. It is possible to say that there is at least one index $\ell^{\dagger\dagger} \in \mathcal{L}_{k^\dagger}$, such that $H^{\ell^{\dagger\dagger}}_{k^\dagger}$ is non-zero. If $\ell^{\dagger\dagger}$ is still an index of a face not matching any fracture, i.e. $\ell^{\dagger\dagger} \in \mathcal{L}^\diamond$, there is a neighboring block $k^{\dagger\dagger} \in \mathcal{K}_{\Gamma_{\ell^{\dagger\dagger}}}$, $k^{\dagger\dagger} \neq k^\dagger$ such that the functional term $\|H^{\ell^{\dagger\dagger}}_{k^\dagger} - H^{\ell^{\dagger\dagger}}_{k^\dagger\dagger}\|_{\mathrm{L}^2(\Gamma_{\ell^{\dagger\dagger}})} > 0$, and thus $z_\xi^T G z_\xi > 0$. If, instead, $\Gamma_{\ell^{\dagger\dagger}}$ lies on a fracture, i.e. $\ell^{\dagger\dagger} \in \mathcal{L}^\star$, then $\|H^{\ell^{\dagger\dagger}}_{k^\dagger} - F_{\varrho(\ell^{\dagger\dagger})}\|_{\mathrm{L}^2(\Gamma_{\ell^{\dagger\dagger}})} > 0$, and consequently $z_\xi^T G z_\xi > 0$ also in this case. Let us now turn the attention to the case *iii*), such that it is now $U^m_i = \psi^m_{F_i,j}$ for a certain index j on a single trace S_m of fracture F_i. Substituting into equation (15), and setting, without loss of generality, $\mathbf{K}_{F_i} = 1$, it is: $\forall j = 1, \ldots, N_{F_i}$

$$0 < (\nabla H_{F_i}, \nabla \varphi_{F_i,j})_{F_i} + \alpha (H_{F_i|_{S_m}}, \varphi_{F_i,j|_{S_m}})_{S_m} = \left\langle \psi^m_{F_i,j}, \varphi_{F_i,j|_{S_m}} \right\rangle_{S_m},$$

and choosing in particular H_{F_i} as a test function, it results

$$0 < \left\langle \psi^m_{F_i,j}, H_{F_i|_{S_m}} \right\rangle_{S_m} \leq \|\psi^m_{F_i,j}\|_{\mathcal{U}^m} \|H_{F_i|_{S_m}}\|_{\mathcal{H}^m_S} \Rightarrow \|H_{F_i|_{S_m}}\|_{\mathcal{H}^m_S} > 0,$$

from which it is possible to deduce that the functional is again non-zero and then $z_\xi^T G z_\xi > 0$. Being G positive semi-definite it is $x^T G x \geq 0$ and $x^T G x = 0$ if and only if $x \in \ker(G)$, see [46]. As a consequence we have that $z_\xi \notin \ker(G)$ for $\xi = 1, \ldots, N_w$. The vector space $\mathcal{Z} = \mathrm{span}\{z_1, \ldots, z_{N_w}\}$ is then a subspace of $\mathrm{Im}(G)$, and each vector $y \in \mathcal{Z}$ can be written as $y = Zv$, for a vector $v \in \mathbb{R}^{N_w}$, $v \neq 0$. Then $v^T Z^T G Z v > 0$, which concludes the proof. □

Theorem 4. *Problem* (23) *has a unique solution* $h^\star = [(h^\star_{\mathcal{D}})^T, (h^\star_F)^T]^T, w^\star = [(q^\star)^T, (u^\star)^T]^T, \lambda^\star$, *such that* $h^\star_{\mathcal{D}}, h^\star_F, q^\star, u^\star$ *correspond to the constrained minimum of problem* (19)-(21).

The proof of Theorem 4 follows from Lemma 3 and from classical arguments of quadratic programming (see Theorem 16.2 in [47]).

5. Numerical Results

This Section is devoted to the presentation of some numerical tests on simple geometrical configurations aimed at showing the viability and convergence properties of the new approach proposed herein. Application of the

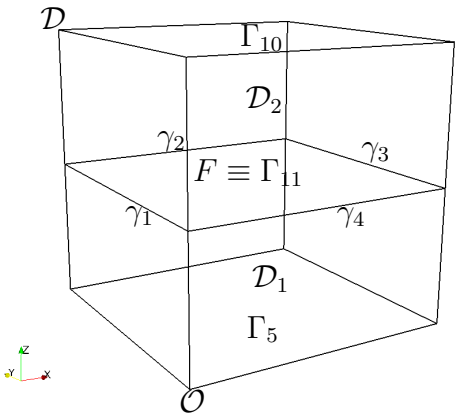

Figure 3: Geometry of test problem T_1 and T_2.

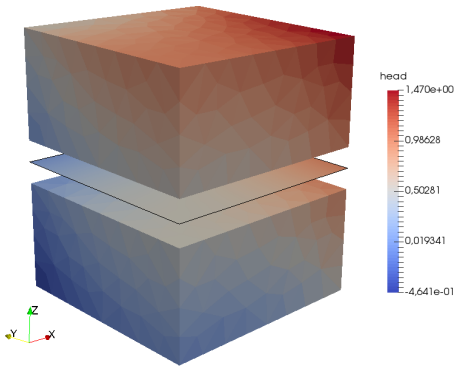

Figure 4: Exploded solution for problem T_1 on grid $\delta = 0.1$.

method to more complex and realistic geometrical settings will be the topic of forthcoming works.

Numerical solutions are obtained on triangular meshes using the BEM on the block faces with element-wise constant basis functions and standard first-order FE on the fractures. The meshes on the fractures are conforming to the meshes on the corresponding block faces for the first four simpler numerical tests reported, whereas the last example considers a more complex configuration and a non-conforming mesh is used. The parameters α and β in definitions (11) and (12) are set to one in the last three problems, and they are set to zero (since not required) in the first two examples. We remark that these two parameters are only required to ensure the well posedness of the problems on fractures or matrix blocks with an empty portion of the Dirichlet boundary, and do not play any other significant role in the behavior of the method. As such the simple choice $\alpha = \beta = 1$ is appropriate in almost all cases. A mesh parameter δ, equal to the square root of the maximum element area, is used to characterize the mesh. The numerical solution of the minimization problem (19)-(21) is obtained solving the KKT system (23). For larger problems the use of a conjugate gradient based solver is recommended, in which the solution is reached through the repeated resolution of small local problems, as done in [7], allowing for a high scalability potential.

5.1. Test problem T_1

As a first example, labeled test problem T_1, let us consider a unit cube $\mathcal{D}$, crossed by a single fracture F parallel to the horizontal faces of the cube and passing through its barycenter, as shown in Figure 3.

A coordinate system centered in $\mathcal{O}$ is chosen, as shown in the figure,

and with reference to it, the face common to the two blocks $\mathcal{D}_1$ and $\mathcal{D}_2$ is labeled Γ_{11}, the bottom face is Γ_5, the top face Γ_{10}, whereas the other faces are labeled counter-clockwise starting, for $\mathcal{D}_1$, from the face parallel to the $x-z$ plane an passing through $\mathcal{O}$, Γ_1, and, for $\mathcal{D}_2$, from face Γ_6, placed on top of Γ_1. The edges of fracture F are labeled as in Figure 3, and we have $\gamma_{F,D} = \gamma_1 \cup \gamma_3$ and $\gamma_{F,N} = \gamma_2 \cup \gamma_4$. The following problem is then set in $\mathcal{D}$:

$$\begin{aligned}
-\mathbf{K}^m \Delta H_1 &= 0, \text{ in } \mathcal{D}_1 && (25)\\
-\mathbf{K}^m \Delta H_2 &= 0, \text{ in } \mathcal{D}_2 && (26)\\
-\mathbf{K}_F \Delta H_F &= -(Q_1^{11} + Q_2^{11}), \text{ in } F && (27)\\
H_1^{11} = H_F &= H_2^{11} && (28)
\end{aligned}$$

with $\mathbf{K}^m = \mathbf{K}_F = 1$, and boundary conditions on the block faces:

$$\begin{aligned}
H_1^5 &= 1/2(x^2 - y^2)\\
H_2^{10} &= 1/2(x^2 - y^2) + 1\\
H_1^2 = H_2^7 &= z - 1/2(1 - y^2)\\
H_1^4 = H_2^9 &= z - 1/2y^2\\
Q_1^1 = Q_2^6 &= 0\\
Q_1^3 = Q_2^8 &= -1
\end{aligned}$$

and on the fracture boundaries:

$$\begin{aligned}
H_{F|_{\gamma_1}} &= 1/2(1 - y^2)\\
H_{F|_{\gamma_3}} &= 1 - 1/2y^2\\
\nabla H_F \cdot \mathbf{n}_{\gamma_2} &= -1\\
\nabla H_F \cdot \mathbf{n}_{\gamma_4} &= 0
\end{aligned}$$

where $\mathbf{n}_{\gamma_i}$ is the outwards unit normal vector to γ_i.

The exact solution to this problem is known and is $H = 1/2(x^2 - y^2) + z$. The numerical approximation computed on a mesh with $\delta = 0.1$ is shown in Figure 4, on an exploded domain, in which it is possible to recognize the two blocks and the fracture plane in between them. Colouring in this figure is proportional to the hydraulic head values. The solution on the fracture plane, h_F, is plotted in Figure 5, and it is represented in grading colours proportional to the value of the hydraulic head. On the same picture the approximated solution h_1^{11} on face Γ_{11} is also shown in light blue, in order to

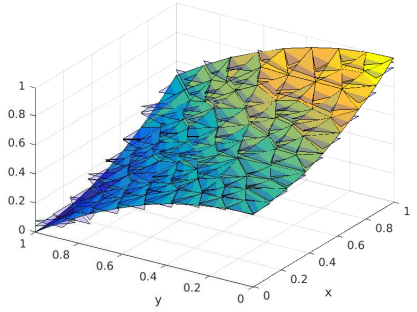

Figure 5: Solution of problem T_1, mesh $\delta = 0.1$ on fracture F (colors proportional to head values) with solution on block $\mathcal{D}_1$ on face Γ_{11} (light blue patches).

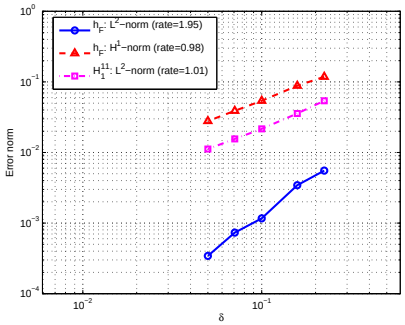

Figure 6: Convergence curves for problem T_1.

highlight the very good agreement with h_F. Error $\|H_{|F} - h_F\|$ is computed in both the $\mathrm{L}^2(F)$ and $\mathrm{H}^1(F)$-norms on the fracture for h_F, whereas the error $\|H_{|\Gamma_{11}} - h_1^{11}\|$ is computed in the $\mathrm{L}^2(\Gamma_{11})$-norm for the piece-wise constant function h_1^{11}. Convergence curves for decreasing values of δ ranging between $0.05 \leq \delta \leq 0.25$ are reported in Figure 6, showing optimal trends for the approximation used. For this first test problem it is possible to compute the conditioning of matrix (23), which ranges from approximately 6.4×10^4 on the coarsest mesh to approximately 7.1×10^7 on the finest mesh. Even if the conditioning can be acceptable for simple problems, we remark again that for larger problems the resolution of the KKT system (23) is not recommended, and iterative preconditioned solvers, such as the preconditioned conjugate gradient method, as proposed in [9] for large scale DFN problems, should be preferred.

5.2. Test problem T_2

The second test problem proposed, labeled T_2, shares the same geometry of T_1, and the same formulation (25)-(28), with different boundary conditions and coefficients. In particular, in this case homogeneous Dirichlet boundary conditions are imposed on Γ_5 and Γ_{10}, whereas homogeneous Neumann boundary conditions are imposed on all the other block faces. A unit head value is imposed on $\gamma_{F,\mathrm{D}} = \gamma_1$, and all other fracture edges are insulated. It can be noticed that the method allows for a great flexibility in the imposition of boundary conditions, as shown by the present example, where a Dirichlet boundary condition is prescribed on a fracture edge surrounded by insulated block faces. This reflects realistic configurations in which, for example, the flow in a matrix block is driven by the presence of the fracture. The value of $\mathbf{K}^m$ is fixed to one, whereas three different values for $\mathbf{K}_F = (1, 10, 100)$ are

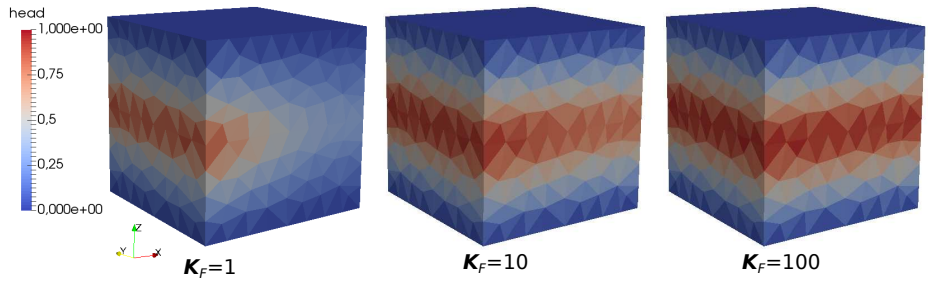

Figure 7: Solution for problem T_2 on a mesh with $\delta = 0.1$ and three values of $\mathbf{K}_F$

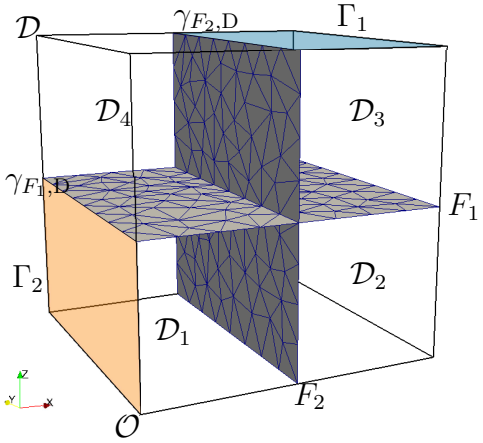

Figure 8: Geometry for test problem T_3

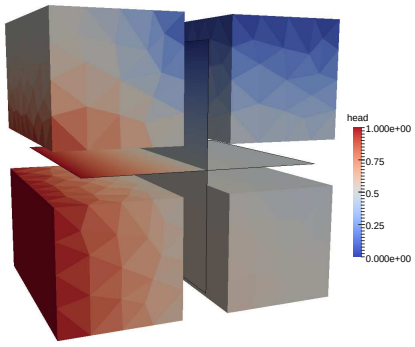

Figure 9: Exploded view of the solution for problem T_3 on a mesh with $\delta = 0.1$.

used for three different simulations, thus prescribing a maximum difference between the matrix permeability and the fracture permeability of two orders of magnitude. Simulations are all performed on a mesh with $\delta = 0.1$. In this setting, then, there is a source of hydraulic head at one edge of the fracture, and a sink is located at the two horizontal faces of the matrix block. The analysis of the results is in this case qualitative: looking at Figure 7, it is possible to see that, at increasing values of $\mathbf{K}_F$ the hydraulic head reaches higher values more in depth of the matrix block, diffusing through the fracture, and this is an expected behavior. Higher differences of permeability between matrix and fractures could also be handled by the method.

5.3. Test problem T_3

The third proposed example, labeled T_3, considers a slightly more complex geometry than the previous problems, with two intersecting fractures immersed in a unit side cube, as shown in Figure 8. With reference to this figure, in addition to the face labels shown therein, Γ_{19} and Γ_{20} are the left and right face on F_1, respectively, whereas Γ_{17} and Γ_{18} are the lower and upper face on F_2, respectively. Problem setting is as in (1)-(2),(4)-(5),(7)-

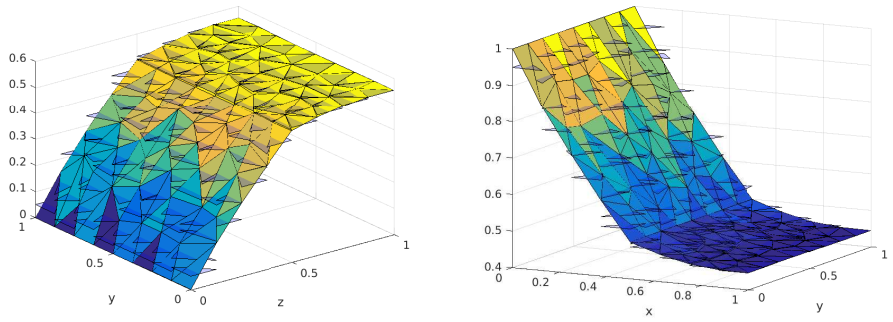

Figure 10: Solution of problem T_3 on the fractures (in grading colors, F_1 left, F_2 right) with solution on the corresponding faces (in light-blue patches, Γ_{17} and Γ_{18}, left, Γ_{19} and Γ_{20}, right).

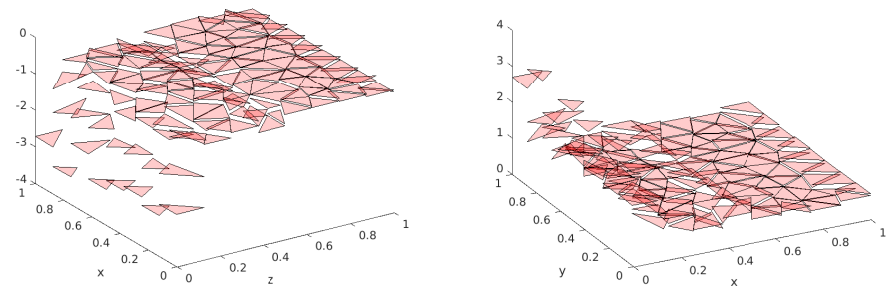

Figure 11: Flux mismatch across fracture F_1 (left) and F_2 (right) for problem T_3.

(8), with $f_k = 0$, $\mathbf{K}_k^m = 1$, $\mathbf{K}_{F_i} = 1$, $i = 1, 2$, and the following boundary conditions: a unitary head is prescribed on face Γ_1 and on the edge of F_2 labeled $\gamma_{F_2,\mathrm{D}}$, null head on Γ_2 and $\gamma_{F_1,\mathrm{D}}$ (see Figure 8 for labels to faces and fracture edges), whereas all other boundary faces and fracture edges are insulated. The obtained solution, on a mesh with parameter $\delta = 0.1$ is shown in Figure 9, with an exploded view. Looking at Figure 10, where the solution on the fractures is reported along with the solution on the matching faces, it can be seen that there is a good agreement between the two. Moreover, as expected, the solution on the fractures has a jump in the first order derivatives along the intersection. We can gain more insight into the quality of the solutions by introducing the following quantities:

$$\Delta h = \sum_{\ell \in \mathcal{L}^\star} \left\| h_k^\ell - h_{F_{\varrho(\ell)}} \right\|_{\mathrm{L}^2(\Gamma_\ell)} + \sum_{\ell \in \mathcal{L}^\diamond} \left\| h_y^\ell - h_z^\ell \right\|_{\mathrm{L}^2(\Gamma_\ell)}$$

Table 3: Values of Δh for problem T_3 for four different mesh parameters δ

δ	0.4	0.2	0.1	0.05
Δh	0.160	0.075	0.038	0.019

and

$$\Delta q = \sum_{\ell \in \mathcal{L}^\diamond} \left\| q_y^\ell + q_z^\ell - \beta \left(h_y^\ell + h_z^\ell \right) \right\|_{\mathrm{L}^2(\Gamma_\ell),}$$

which can be regarded as two error indicators. In particular, Δh is a measure of the continuity error of the solution at fracture-block interfaces, i.e. on the faces Γ_ℓ with $\ell \in \mathcal{L}^\star$, and at block-block interfaces, i.e. on the faces Γ_ℓ with $\ell \in \mathcal{L}^\diamond$; Δq is a measure of flux unbalance at block-block interfaces. Concerning problem T_3, we have that $\mathcal{L}^\diamond = \emptyset$, and consequently Δq is zero, and Δh represents the error in the continuity of the solution at the fracture-block interfaces. The values for Δh obtained on four different meshes are reported in Table 3. It can be seen that, as expected, there is a clear decreasing trend for Δh as the mesh parameter δ is reduced.

Finally, Figure 11 shows the mismatch of the co-normal derivative of the solution on the matrix blocks across the fractures, which corresponds to the forcing terms of the problems on the fractures. Thus it can be concluded that the solution displays the expected behavior.

5.4. Test problem T_4

This example, labeled problem T_4, shows the behavior of the method in the case of a network of fractures completely immersed in the matrix, i.e. without any fracture hitting the boundary of the computational domain. The domain $\mathcal{D}$ for this problem is shown in Figure 5, and it consists of two square-shaped intersecting fractures with unit size edge, immersed in a cubical block with edge size 1.2.

The domain is split into five blocks $\mathcal{D}_k$, $k = 1, \ldots, 5$, and in particular, block $\mathcal{D}_5$ is a cube with a cubic cavity hosting the remaining blocks $\mathcal{D}_1$-$\mathcal{D}_4$, which, in turn, surround the two fractures F_1 and F_2. Dirichlet boundary conditions are prescribed on a portion of the top and bottom face of $\mathcal{D}$ (see the shaded areas in Figure 5), with a prescribed value of head equal to one on the bottom face and equal to zero on the top face. All other edges are insulated. Concerning the fractures, a no flow boundary condition is imposed at fracture borders, as a consequence of the vanishing aperture of the fractures at their borders. The transmissivity of the matrix blocks is equal to one, whereas the transmissivity of fractures is set to $\mathbf{K}_{F_1} = \mathbf{K}_{F_2} := \mathbf{K}_F = 10^3$. The solution on the outer faces of block $\mathcal{D}_5$ is shown in Figure 5.

Figure 5 displays the solution on the faces of blocks $\mathcal{D}_1$-$\mathcal{D}_4$, and in transparency the solution on the two fractures, along with the computing mesh.

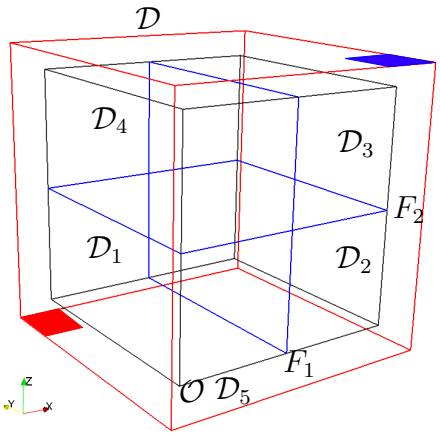

Figure 12: Geometry of problem T_4 and boundary conditions

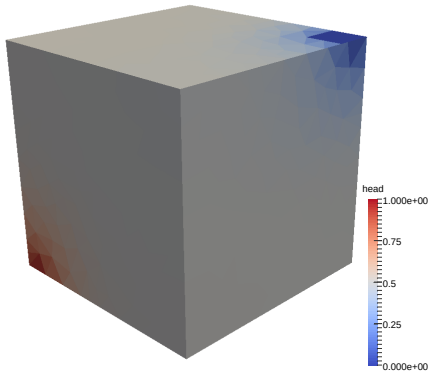

Figure 13: Solution on the external faces of block $\mathcal{D}_5$ for problem T_4 on a mesh with $\delta = 0.1$

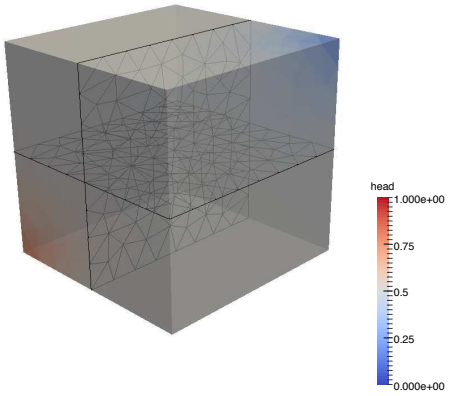

Figure 14: Solution of problem T_4 on the external faces of blocks $\mathcal{D}_1$-$\mathcal{D}_4$, and, in transparency, on the fractures. Mesh with $\delta = 0.1$.

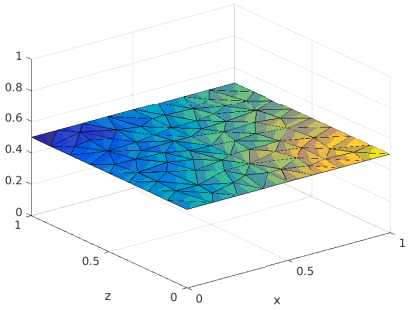

Figure 15: Solution of problem T_4 on fracture F_1, mesh $\delta = 0.1$

Table 4: Values of Δh and Δq for problem T_4 for three different mesh parameters δ and two values of $\mathbf{K}_F$

	$\mathbf{K}_F = 10^3$		$\mathbf{K}_F = 1$	
δ	Δh	Δq	Δh	Δq
0.4	1.0×10^{-5}	4.5×10^{-10}	6.7×10^{-3}	2.1×10^{-4}
0.2	5.6×10^{-6}	1.7×10^{-10}	3.3×10^{-3}	6.1×10^{-5}
0.1	3.0×10^{-6}	4.8×10^{-11}	1.7×10^{-3}	1.6×10^{-5}

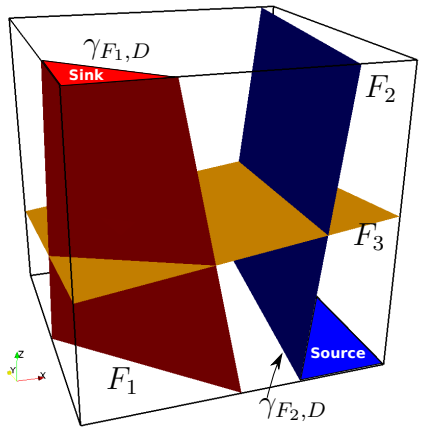

Figure 16: Geometry of problem T_5 with boundary conditions

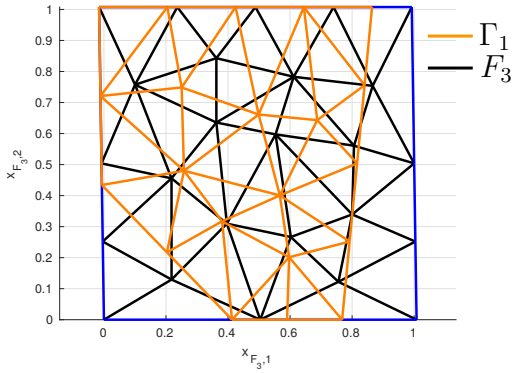

Figure 17: Detail of the meshes ($\delta = 0.2$) on fracture F_3 and face Γ_1 for problem T_5

It can be noticed that the solution on and around the fractures is almost constant, (see also Figure 15) as a consequence of the high value of the transmissivity of the fractures with respect to the transmissivity of the matrix. Let us observe that, in this case, block-block interfaces are present, i.e. the set $\mathcal{L}^\diamond \neq \emptyset$, thus Table 4 reports the values of both Δh e Δq at refinement of the mesh parameter δ. The considered case with $\mathbf{K}_F = 10^3$ is shown along with the results obtained in the case $\mathbf{K}_F = 1$, being the transmissivity of the matrix equal to one in both cases. It can be seen that, as expected, both the considered error indicators have a clear converging trend. The lower values of Δh, if compared to those of problem T_3, are due to the fact that the solution of problem T_4 has a lower gradient, and, for the same reason the values related to problem T_4 corresponding to $\mathbf{K}_F = 10^3$ are lower than the values for $\mathbf{K}_F = 1$. The proposed results confirm the correct behavior of the method, also in this configuration.

5.5. Test problem T_5

In this last example a more complex geometry is considered, with three fractures, having general spatial orientation, crossing a unit cube, as shown

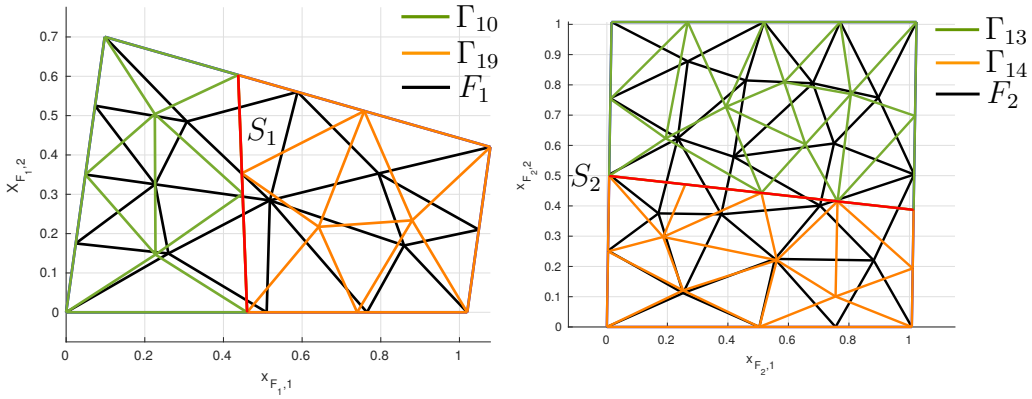

Figure 18: Detail of the meshes ($\delta = 0.2$) on fracture F_1 (left) and F_2 (right) and on the matching block faces

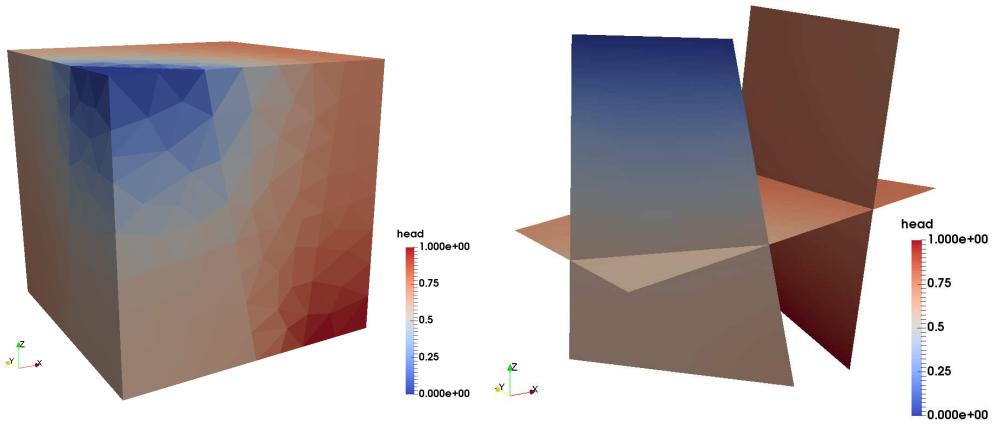

Figure 19: Solution of problem T_5 in the matrix block (left) and on the immersed DFN (right), mesh $\delta = 0.1$

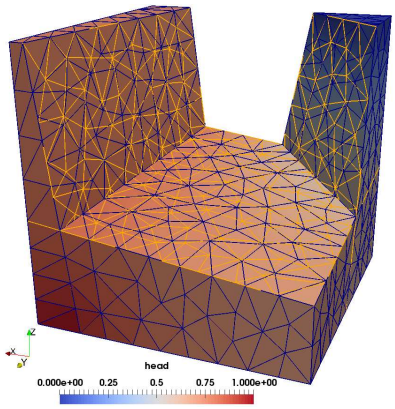

Figure 20: Solution of problem T_5 on the fracture network and on some of the blocks, mesh $\delta = 0.1$

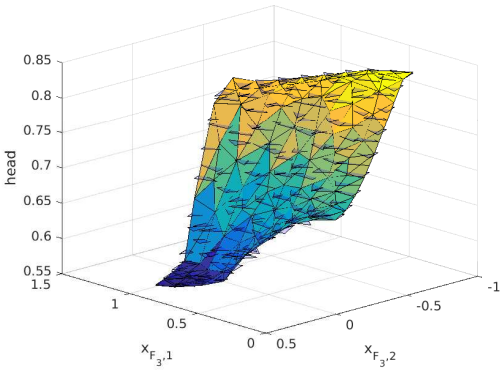

Figure 21: Solution of problem T_5 on fracture F_3, mesh $\delta = 0.1$

in Figure 5. Boundary conditions are prescribed on two boundary faces, as shown in the figure, setting a fixed head drop equal to one between the source face and the sink face. The same pressure drop is set between the fracture edges $\gamma_{F_2,D}$ and $\gamma_{F_1,D}$, whereas all other fracture edges and block faces are insulated. The hydraulic transmissivity is set to one for both the fractures and the matrix. The mesh for this example is non-conforming: namely, the mesh on the fractures is non-conforming to both the intersections with the other fractures and to the mesh on the matching block faces, as shown in Figures 5-5. In Figure 5 the mesh of fracture F_3 is displayed, along with the mesh on one of the matching faces, whereas in Figure 5 the mesh on fractures F_1 and F_2, respectively, is plotted along with the mesh on the matching faces. It can be seen that the meshes on the block faces are also not conforming at the traces. The computed solution on a mesh with $\delta = 0.1$ is reported in Figure 5, where the solution on the outer faces of the matrix is shown on the left, with coloring proportional to the hydraulic head, and the solution on the immersed fracture network is reported on the right, with the same color legend. Figure 5 reports the same computed solution, where one of the matrix blocks has been removed in order to show the solution inside. We can see that the solution on the fractures well matches the solution on the surrounding matrix blocks. In Figure 5, the non-conforming meshes can also be seen. Figure 5 reports the solution computed on fracture F_3, along with the solution on the matching faces, shown in light blue patches, to highlight the good matching between the two. The behavior of the error indicator Δh is finally reported in Table 5, to give a more quantitative insight on the quality of the solution: it can be seen that as the mesh is refined the error

Table 5: Values of Δh for three different mesh parameters δ

δ	0.4	0.2	0.1
Δh	0.185	0.094	0.046

indicator reduces.

6. Conclusions

A new formulation for the simulation of the flow in poro-fractured domains is presented, based on an optimization approach. The three dimensional Darcy law in the porous matrix and the coupled reduced Darcy law on the fractures is solved resorting to the minimization of a properly designed cost functional for the imposition of matching conditions at fracture-matrix and fracture-fracture interfaces. The method relaxes the mesh matching constraints at the interfaces, thus paving the way to an easy and reliable meshing process, as already done in previous works in the context of discrete fracture network flow simulations. Moreover, the optimization approach allows for the decoupling of the original problem into smaller problems, thus providing a high scalability potential, which is a crucial aspect for computationally demanding simulations. In this work the well posedness of the optimization formulation is stated, both in a continuous and discrete framework. Numerical results on simple three-dimensional problems show the expected convergence properties for the proposed method and prove its viability for simulating underground flows in poro-fractured media.

Acknowledgments

This work has been partially supported by INdAM-GNCS and by Politecnico di Torino through project "Starting Grant RTD". Computational resources were partially provided by HPC@POLITO computational facility of Politecnico di Torino (http://hpc.polito.it).

Appendix A.

The following is devoted to a precise definition of the matrices involved in the previous statements. This is done using the Boundary Element Method (BEM) on the matrix blocks and standard first order Finite Elements on the fracture faces. We will assume that the source term f in the matrices is zero, the extension to the general case being straightforward. For this reason, both vectors $b_{\mathcal{D}}$ and b_F only account for boundary conditions. Furthermore, for the sake of simplicity we assume that the matrix trasmissivity is constant on each block, i.e. $\mathbf{K}_k^m = K_k^m$, $k = 1, \ldots, n_{\mathcal{D}}$.

Appendix A.1. Assembling $A_{\mathcal{D}}$, $\mathcal{B}^q$ and b

The Boundary Element Method (BEM) for the numerical resolution of equation (14) provides the definition of h on the boundaries of each matrix block $\mathcal{D}_k$. Let us denote by $\chi_k(\mathbf{x}, \mathbf{x}_0)$ the Green function of the operator $-K_k^m \Delta(\cdot)$ in 3D, defined as

$$\chi_k(\mathbf{x}, \mathbf{x}_0) = \frac{1}{4K_k^m \pi \|\mathbf{x} - \mathbf{x}_0\|}$$

with $\|\cdot\|$ the Euclidean norm in $\mathbb{R}^3$. Let us fix a block index k, and let us introduce for the basis functions $\phi_{k,j}^{\ell}$, $j = 1, \ldots, N_k^{\Gamma_\ell}$, $\ell \in \mathcal{L}_k$ a global numbering: $\phi_{k,\zeta}$, $\zeta = 1, \ldots, N_k$. We then set:

$$H_k = \sum_{j=1}^{N_k} h_{k,j} \phi_{k,j}(\mathbf{x}), \qquad Q_k = \sum_{j=1}^{N_k} q_{k,j} \phi_{k,j}(\mathbf{x}).$$

Furthermore, let us introduce, for each $k = 1, \ldots, n_{\mathcal{D}}$ a set of nodes $(\mathbf{x}_{k,j})_{j=1,\ldots,N_k}$ in $\mathcal{D}_k$ and, without loss of generality basis functions are such that exists $\mathbf{x}_{k,j}$ providing $\phi_{k,i}(\mathbf{x}_{k,j}) = \delta_{i,j}$, $i, j = 1, \ldots, N_k$. For each internal block, i.e. for each $\mathcal{D}_k$ such that $\mathcal{L}_k \cap \mathcal{L}_{\partial\mathcal{D}} = \emptyset$, we have that:

$$\frac{1}{2} h_{k,j} = \int_{\partial\mathcal{D}_k} (Q_k(\mathbf{x}) - \beta H_k(\mathbf{x})) \chi_k(\mathbf{x}, \mathbf{x}_j) - \int_{\partial\mathcal{D}_k} H_k(\mathbf{x}) \left(K_k^m \nabla \chi_k(\mathbf{x}, \mathbf{x}_j) \cdot \mathbf{n}_{\partial\mathcal{D}_k}\right).$$

We then collect integrals into matrices $A_k, \mathcal{B}_k^q \in \mathbb{R}^{N_k \times N_k}$ defined as follows:

$$(A_k)_{j,i} = \int_{\partial\mathcal{D}_k} \beta \phi_{k,i}(\mathbf{x})) \chi_k(\mathbf{x}, \mathbf{x}_j) + \int_{\partial\mathcal{D}_k} \phi_{k,i}(\mathbf{x}) \left(K_k^m \nabla \chi_k(\mathbf{x}, \mathbf{x}_j) \cdot \mathbf{n}_{\partial\mathcal{D}_k}\right) + \frac{1}{2}\delta_{ij}, \tag{A.1}$$

$$(\mathcal{B}_k^q)_{j,i} = \int_{\partial\mathcal{D}_k} \phi_{k,i}(\mathbf{x}) \chi_k(\mathbf{x}, \mathbf{x}_j). \tag{A.2}$$

For boundary blocks, i.e. for all $k = 1, \ldots, n_{\mathcal{D}}$ such that $\mathcal{L}_k \cap \mathcal{L}_{\partial\mathcal{D}} \neq \emptyset$, without loosing generality, we can assume that boundary faces carrying Dirichlet boundary conditions, correspond to the first face indexes in $\mathcal{L}_k$, and consequently the coefficients and the basis functions of H_k^{ℓ} for $\ell \in \mathcal{L}_k \cap \mathcal{L}_{\partial\mathcal{D}}$ occupy the first N_k^* positions in h_k. We denote by $H_k^{\mathrm{D}} = \sum_{j=1}^{N_k^*} h_{k,j}^{\mathrm{D}} \phi_{k,j}(\mathbf{x})$ the (known) part of H_k, corresponding to the Dirichlet faces, being $h_{k,j}^{\mathrm{D}}$ known coefficients deriving from the discretization of the boundary conditions, collected in the column vector h_k^{D}. Instead $H_k^* = \sum_{j=N_k^*+1}^{N_k} h_{k,j} \phi_{k,j}(\mathbf{x})$ is the remaining (unknown) part of H_k.

Thus, for boundary blocks, it is: for $j = 1, \ldots, N_k$, $i = 1, \ldots, N_k^*$

$$(A_k)_{j,i} = \int_{\partial \mathcal{D}_k} \phi_{k,i}(\mathbf{x}) \chi_k(\mathbf{x}, \mathbf{x}_j),$$

$$(\mathcal{B}_k)_{j,i} = K_k^m \int_{\partial \mathcal{D}_k} \phi_{k,i}(\mathbf{x}) \left(\nabla \chi_k(\mathbf{x}, \mathbf{x}_j) \cdot \mathbf{n}_{\partial \mathcal{D}_k}\right) + \frac{1}{2}\delta_{ij},$$

whereas for $j = 1, \ldots, N_k$, $i = N_k^* + 1, \ldots, N_k$, $(A_k)_{j,i}$ is as in (A.1), and $(\mathcal{B}_k^q)_{j,i}$ is as in (A.2).

Finally we have that

$$A_{\mathcal{D}} = \mathrm{diag}(A_k, k = 1, \ldots, n_{\mathcal{D}}), \qquad \mathcal{B}^q = \mathrm{diag}(\mathcal{B}_k^q, k = 1, \ldots, n_{\mathcal{D}}),$$

and

$$b_k = \mathcal{B}_k h_k^{\mathrm{D}}, \qquad b_{\mathcal{D}} = \begin{bmatrix} b_1 \\ \vdots \\ b_k \\ \vdots \\ b_{n_{\mathcal{D}}} \end{bmatrix}.$$

Appendix A.2. Assembling A_F, $\mathcal{B}^u$, $\mathcal{B}_F^q$ and B_F

Let us introduce matrices $A_{F_i} \in \mathbb{R}^{N_{F_i} \times N_{F_i}}$ defined as:

$$(A_{F_i})_{pz} = \int_{F_i} \mathbf{K}_{F_i} \nabla \varphi_{F_i,p} \nabla \varphi_{F_i,z}, \qquad i = 1, \ldots, I,$$

and we then have $A_F = \mathrm{diag}(A_{F_i}, i = 1, \ldots, I)$. Furthermore, let us set matrices $\mathcal{B}_{F_i,F_i,S_m} \in \mathbb{R}^{N^{F_i} \times N_{F_i}^{S_m}}$, for $i = 1, \ldots, I$ and $S_m \in \mathcal{S}_i$ as:

$$(\mathcal{B}_{F_i,F_i,S_m})_{p,z} = \int_{S_m} \varphi_{F_i,p} \psi_{F_i,z}^m.$$

The repeated subscript F_i in $\mathcal{B}_{F_i,F_i,S_m}$ is used here to distinguish these matrices from matrices $\mathcal{B}_{F_i,F_j,S_m}$ introduced later in this Appendix. Matrices $\mathcal{B}_{F_i,F_i,S_m}$ are grouped row-wise for increasing values of m such that $S_m \in \mathcal{S}_i$ to form matrices $\mathcal{B}_{F_i}^u \in \mathbb{R}^{N_{F_i} \times N_{F_i}^{\mathcal{S}_i}}$. Matrices $\mathcal{R}_{F_i} \in \mathbb{R}^{N^{\mathcal{S}} \times N_{F_i}^{\mathcal{S}_i}}$, instead, represent the action of an operator that extracts from vector u sub-vectors u_i for $i = 1, \ldots, I$, i.e. $u_i = \mathcal{R}_{F_i} u$, and then we set:

$$\mathcal{B}^u \in \mathbb{R}^{N_F \times N^{\mathcal{S}}}, \qquad \mathcal{B}^u = \begin{bmatrix} \mathcal{B}_{F_1}^u \mathcal{R}_{F_1} \\ \vdots \\ \mathcal{B}_{F_I}^u \mathcal{R}_{F_I} \end{bmatrix}.$$

Let us denote by $\mathcal{B}^q_{F_i,k,\Gamma_\ell} \in \mathbb{R}^{N_{F_i} \times N_k^{\Gamma_\ell}}$ the matrix defined for $i = 1, \ldots, I$ as:

$$\begin{aligned}(\mathcal{B}^q_{F_i,k,\Gamma_\ell})_{p,z} = &\int_{\Gamma_\ell} \phi^\ell_{k,z}(\sigma_i(\mathbf{x}))\varphi_{F_i,p}(\mathbf{x}_{F_i}), \quad \ell \in \mathcal{L}_{F_i},\ k \in \mathcal{K}_{\Gamma_\ell}\\ (\mathcal{B}^q_{F_i,k,\Gamma_\ell})_{p,z} = &\qquad 0, \qquad\qquad\qquad \ell \notin \mathcal{L}_{F_i},\ k \in \mathcal{K}_{\Gamma_\ell}\end{aligned}$$

where $\sigma_i(\mathbf{x})$ is used to denote a mapping from the 3D reference system restricted to Γ_ℓ to the 2D reference system on F_i, which is actually a rotation and translation. For each $i = 1, \ldots, I$, let us denote by $\mathcal{K}_{F_i}$ the set of matrix block indexes having one face on F_i, i.e. $\mathcal{K}_{F_i} = \bigcup_{\ell \in \mathcal{L}_{F_i}} \mathcal{K}_{\Gamma_\ell}$. We now collect, for each $i = 1, \ldots, I$, matrices $\mathcal{B}^q_{F_i,k,\Gamma_\ell}$ row-wise to form the new matrices $\mathcal{B}^q_{F_i} \in \mathbb{R}^{N_{F_i} \times N_{\mathcal{D}}}$ in the following way: for all $k = 1, \ldots, n_{\mathcal{D}}$

$$\mathcal{B}^q_{F_i,k} = \left[\begin{array}{cccc} \mathcal{B}^q_{F_i,k,\Gamma_{\ell_1}} & \mathcal{B}^q_{F_i,k,\Gamma_{\ell_2}} & \cdots & \mathcal{B}^q_{F_i,k,\Gamma_{\ell_{n_k}}} \end{array}\right], \qquad \ell_1 < \ell_2 < \cdots < \ell_{n_k} \in \mathcal{L}_k,$$

$$\mathcal{B}^q_{F_i} = \left[\begin{array}{ccc} \mathcal{B}^q_{F_i,1} & \cdots & \mathcal{B}^q_{F_i,n_{\mathcal{D}}} \end{array}\right],$$

with n_k the number of elements of $\mathcal{L}_k$.

Finally matrix $\mathcal{B}^q_F \in \mathbb{R}^{N_F \times N_{\mathcal{D}}}$ is obtained grouping column-wise matrices $\mathcal{B}^q_{F_i}$ for increasing values of $i = 1, \ldots, I$.

Let us now define, for $m = 1, \ldots, M$ and $i, j \in \mathcal{I}_{S_m}$, $i \neq j$, matrices $\mathcal{B}_{F_i,F_j,S_m} \in \mathbb{R}^{N_{F_i} \times N_{F_j}^{S_m}}$ as follows:

$$(\mathcal{B}_{F_i,F_j,S_m})_{p,z} = \int_{S_m} \varphi_{F_i,p}\psi^m_{F_j,z},$$

and matrices $B_{F_i,S_m} \in \mathbb{R}^{N_{F_i} \times N^{S_m}}$ as: for $i = 1, \ldots, I$, $S_m \in \mathcal{S}_i$, $p, z \in \mathcal{I}_{S_m}$ with $p < z$ (i.e. $p = i$ or $z = i$):

$$B_{F_i,S_m} = [\mathcal{B}_{F_i,F_p,S_m},\ \mathcal{B}_{F_i,F_z,S_m}],$$

which are then grouped row-wise to form matrices $B_{F_i} \in \mathbb{R}^{N_{F_i} \times N^{\mathcal{S}_i}}$ for increasing values of m such that $S_m \in \mathcal{S}_i$. Then, let $R_{F_i} \in \mathbb{R}^{N^{\mathcal{S}} \times N^{\mathcal{S}_i}}$ be a matrix representing the action of an operator that extracts from vector u sub-vectors u_i^+ for $i = 1, \ldots, I$, i.e. $u_i^+ = R_{F_i}u$. Matrix $B_F \in \mathbb{R}^{N_F \times N^{\mathcal{S}}}$ is finally given by:

$$B_F = \left[\begin{array}{c} B_{F_1}R_{F_1} \\ \vdots \\ B_{F_I}R_{F_I} \end{array}\right].$$

Appendix A.3. Assembling matrices $G^h_{\mathcal{D},\mathcal{D}}$, $\mathcal{B}^h_F$ and $G^h_{F,F}$

Let us start by introducing matrices $G_{k,k,\Gamma_\ell} \in \mathbb{R}^{N_k^{\Gamma_\ell} \times N_k^{\Gamma_\ell}}$, $G_{k,y,\Gamma_\ell} \in \mathbb{R}^{N_k^{\Gamma_\ell} \times N_y^{\Gamma_\ell}}$, and $G_{k,F_i,\Gamma_\ell} \in \mathbb{R}^{N_k^{\Gamma_\ell} \times N_{F_i}}$, defined respectively as:

$$(G_{k,k,\Gamma_\ell})_{p,z} = \tilde{\beta} \int_{\Gamma_\ell} \phi^\ell_{k,p}(\mathbf{x})\phi^\ell_{k,z}(\mathbf{x}), \quad \forall \ell \in \mathcal{L}_\mathcal{D}, \quad \tilde{\beta} = \begin{cases} 1 & \ell \in \mathcal{L}^\star, \\ 1+\beta^2 & \ell \in \mathcal{L}^\diamond, \end{cases}$$

$$G_{k,k,\Gamma_\ell} = 0, \quad \forall \ell \in \mathcal{L}_{\partial\mathcal{D}}, \quad k \in \mathcal{K}_{\Gamma_\ell};$$

$$(G_{k,y,\Gamma_\ell})_{p,z} = (\beta^2 - 1) \int_{\Gamma_\ell} \phi^\ell_{k,p}(\mathbf{x})\phi^\ell_{y,z}(\mathbf{x}), \quad \forall \ell \in \mathcal{L}^\diamond,\ k, y \in \mathcal{K}_{\Gamma_\ell},\ k \neq y;$$

$$G_{k,y,\Gamma_\ell} = 0, \qquad \forall \ell \in \mathcal{L}^\diamond,\ k \in \mathcal{K}_{\Gamma_\ell},\ y \notin \mathcal{K}_{\Gamma_\ell};$$

$$G_{k,y,\Gamma_\ell} = 0, \qquad \forall \ell \in \mathcal{L}^\star,\ k, y \in \mathcal{K}_{\Gamma_\ell}, k \neq y;$$

$$(G_{k,F_i,\Gamma_\ell})_{p,z} = \int_{\Gamma_\ell} \phi^\ell_{k,p}(\sigma_i(\mathbf{x}))\varphi^\ell_{F_i,z}(\mathbf{x}_{F_i}), \qquad \forall \ell \in \mathcal{L}^\star, k \in \mathcal{K}_{\Gamma_\ell},\ i = \varrho(\ell),$$

and $G_{k,F_i,\Gamma_\ell} = 0$, otherwise.

With these matrices we build for $k = 1, \ldots, n_\mathcal{D}$, $\ell_1 < \ell_2 < \ldots < \ell_{n_k} \in \mathcal{L}_k$ and $y \in \mathcal{K}_{\Gamma_{\ell_r}}$, $y \neq k$:

$$G_{k,k} = \mathrm{diag}(G_{k,k,\Gamma_{\ell_r}}, r = 1, \ldots, n_k), \quad G_{k,y} = \mathrm{diag}(G_{k,y,\Gamma_{\ell_r}}, r = 1, \ldots, n_k)$$

and then we set $G_k = G_{k,k} + G_{k,y}$. Also for $k = 1, \ldots, n_\mathcal{D}$ and $i = 1, \ldots, I$, we define matrices

$$G_{k,F,\Gamma_\ell} = \begin{bmatrix} G_{k,F_1,\Gamma_\ell} & \cdots & G_{k,F_i,\Gamma_\ell} & \cdots & G_{k,F_I,\Gamma_\ell} \end{bmatrix}.$$

Matrix $G^h_{\mathcal{D},\mathcal{D}}$ is then obtained collecting column-wise matrices G_k, whereas matrices G_{k,F,Γ_ℓ} are grouped column wise for increasing values of $\ell \in \mathcal{L}_k$ to form matrices

$$G_{k,F} = \begin{bmatrix} G_{k,F,\Gamma_{\ell_1}} \\ \vdots \\ G_{k,F,\Gamma_{\ell_r}} \\ \vdots \\ G_{k,F,\Gamma_{\ell_{n_k}}} \end{bmatrix}, \qquad \ell_1 < \ell_2 < \ldots < \ell_{n_k} \in \mathcal{L}_k.$$

Finally we have

$$G^h_{\mathcal{D},F} = \begin{bmatrix} G_{1,F} \\ \vdots \\ G_{k,F} \\ \vdots \\ G_{n_\mathcal{D},F} \end{bmatrix} \in \mathbb{R}^{N_\mathcal{D} \times N_F}, \qquad \mathcal{B}^h_F = (G^h_{\mathcal{D},F})^T.$$

Furthermore, being

$$(G_{F_i,F_i})_{p,z} = \int_{F_i} \varphi_{F_i,p}(\mathbf{x}_{F_i})\varphi_{F_i,z}(\mathbf{x}_{F_i}), \quad \forall i = 1,\dots,I,$$

matrix $G^h_{F,F} \in \mathbb{R}^{N_F \times N_F}$ is defined as:

$$G^h_{F,F} = \mathrm{diag}(G_{F_i,F_i}, i = 1\dots,I).$$

Appendix A.4. Assembling matrix G^h_F

Let us introduce matrices $C_{F_i,F_i} \in \mathbb{R}^{N_{F_i} \times N_{F_i}}$ as:

$$(C_{F_i,F_i,S_m})_{p,z} = (1+\alpha^2) \sum_{S_m \in \mathcal{S}_i} \int_{S_m} \varphi_{F_i,p|_{S_m}} \varphi_{F_j,z|_{S_m}}.$$

For each fracture F_i, for each fracture F_j, $j = 1,\dots,I$, $j \neq i$ we also have matrices $C^{S_m}_{F_i,F_j} \in \mathbb{R}^{N_{F_i} \times N_{F_j}}$, defined as follows:

$$(C_{F_i,F_j,S_m})_{p,z} = \begin{cases} (\alpha^2-1) \displaystyle\int_{S_m} \varphi_{F_i,p|_{S_m}} \varphi_{F_j,z|_{S_m}}, & \text{if } \exists\, m \text{ s.t. } S_m = \bar{F}_i \cap \bar{F}_j \\ 0, & \text{if } \nexists\, m \text{ s.t. } S_m = \bar{F}_i \cap \bar{F}_j \end{cases}$$

which are then grouped block-wise to form matrix $C^h_F \in \mathbb{R}^{N_F \times N_F}$ as follows: for $i = 1,...,I$, for $j = 1,...,I$

$$C_i = \begin{bmatrix} C_{F_i,F_1} & \cdots & C_{F_i,F_j} & \cdots & C_{F_i,F_I} \end{bmatrix}; \quad G^h_F = \begin{bmatrix} C_1 \\ \vdots \\ C_i \\ \vdots \\ C_I \end{bmatrix}.$$

Appendix A.5. Assembling matrices G^u and G^q

Let us now introduce matrix $G^u \in \mathbb{R}^{N^{\mathcal{S}} \times N^{\mathcal{S}}}$ defined as follows:

$$G^u = \mathrm{diag}(\mathcal{C}_{S_m}, m = 1\dots,M),$$

being

$$\mathcal{C}_{S_m} = \begin{bmatrix} \mathcal{C}_{F_i,S_m} & \mathcal{C}_{F_i,F_j,S_m} \\ (\mathcal{C}_{F_i,F_j,S_m})^T & \mathcal{C}^j_{F_j,S_m} \end{bmatrix}, \text{ for } i,j \in \mathcal{I}_{S_m}, i < j,$$

where matrices $\mathcal{C}_{F_i,S_m} \in \mathbb{R}^{N^{S_m}_{F_i}}$, $\mathcal{C}_{F_j,S_m} \in \mathbb{R}^{N^{S_m}_{F_j}}$ and $\mathcal{C}_{F_i,F_j,S_m}$ for $i,j \in \mathcal{I}_{S_m}$ are:

$$(\mathcal{C}_{F_i,S_m})_{p,z} = \int_{S_m} \psi^m_{F_i,p}\psi^m_{F_i,z}, \qquad (\mathcal{C}_{F_i,F_j,S_m})_{p,z} = \int_{S_m} \psi^m_{F_i,p}\psi^m_{F_j,z}.$$

Further for $\ell \in \mathcal{L}_{\mathcal{D}}$ and $k, y \in \mathcal{K}_{\Gamma_\ell}$, possibly $k = y$, we introduce matrices $\mathcal{C}_{k,y,\Gamma_\ell} \in \mathbb{R}^{N_k^{\Gamma_\ell} \times N_y^{\Gamma_\ell}}$ as:

$$(\mathcal{C}_{k,y,\Gamma_\ell})_{p,z} = \int_{\Gamma_\ell} \phi_{k,p}^{\ell}(\mathbf{x}) \phi_{y,z}^{\ell}(\mathbf{x}), \quad \forall \ell \in \mathcal{L}^{\diamond},\ k, y \in \mathcal{K}_{\Gamma_\ell}$$

$\mathcal{C}_{k,y,\Gamma_\ell} = 0,\ \forall \ell \in \mathcal{L}^{\diamond},\ k \in \mathcal{K}_{\Gamma_\ell},\ y \notin \mathcal{K}_{\Gamma_\ell}, \quad \mathcal{C}_{k,y,\Gamma_\ell} = 0,\ \forall \ell \in \mathcal{L}^{\star},\ k, y \in \mathcal{K}_{\Gamma_\ell}, k \neq y,$ which are then grouped for $k = 1, \ldots, n_{\mathcal{D}},\ \ell_1 < \ell_2 < \ldots < \ell_{n_k} \in \mathcal{L}_k$ and $y \in \mathcal{K}_{\Gamma_{\ell_i}},\ y \neq k$ to build matrices:

$$\mathcal{C}_{k,k} = \mathrm{diag}(\mathcal{C}_{k,k,\Gamma_{\ell_r}}, r = 1, \ldots, n_k), \quad \mathcal{C}_{k,y} = \mathrm{diag}(\mathcal{C}_{k,y,\Gamma_{\ell_r}}, r = 1, \ldots, n_k)$$

and then $G_k^q = \mathcal{C}_{k,k} + \mathcal{C}_{k,y} \in \mathbb{R}^{N_k \times N_{\mathcal{D}}}$, $k = 1, \ldots, n_{\mathcal{D}}$. Matrix $G^q \in \mathbb{R}^{N_{\mathcal{D}} \times N_{\mathcal{D}}}$ is then obtained grouping matrices G_k^q column-wise for increasing values of k.

References

[1] C. Alboin, J. Jaffré, J. E. Roberts, C. Serres, Modeling fractures as interfaces for flow and transport in porous media, in: Z. Chen, R. E. Ewing (Eds.), Fluid Flow and Transport in Porous Media: Mathematical and Numerical Treatment, Vol. 295 of Contemporary Mathematics, American Mathematical Society, Providence, RI USA, 2002, pp. 13–24.

[2] V. Martin, J. Jaffré, J. E. Roberts, Modeling fractures and barriers as interfaces for flow in porous media, SIAM Journal on Scientific Computing 26 (5) (2005) 1667–1691. doi:10.1137/S1064827503429363.

[3] S. Berrone, S. Pieraccini, S. Scialò, A PDE-constrained optimization formulation for discrete fracture network flows, SIAM J. Sci. Comput. 35 (2) (2013) B487–B510. doi:http://dx.doi.org/10.1137/120865884.

[4] S. Berrone, S. Pieraccini, S. Scialò, On simulations of discrete fracture network flows with an optimization-based extended finite element method, SIAM J. Sci. Comput. 35 (2) (2013) A908–A935. doi:http://dx.doi.org/10.1137/120882883.

[5] S. Berrone, S. Pieraccini, S. Scialò, An optimization approach for large scale simulations of discrete fracture network flows, J. Comput. Phys. 256 (2014) 838–853. doi:http://dx.doi.org/10.1016/j.jcp.2013.09.028.

[6] M. Benedetto, S. Berrone, S. Pieraccini, S. Scialò, The virtual element method for discrete fracture network simulations, Comput. Methods Appl. Mech. Engrg. 280 (0) (2014) 135 – 156. doi:http://dx.doi.org/10.1016/j.cma.2014.07.016.

[7] S. Berrone, S. Pieraccini, S. Scialò, F. Vicini, A parallel solver for large scale DFN flow simulations, SIAM J. Sci. Comput. 37 (3) (2015) C285–C306. doi:http://dx.doi.org/10.1137/140984014.

[8] S. Berrone, A. Borio, S. Scialò, A posteriori error estimate for a PDE-constrained optimization formulation for the flow in DFNs, SIAM J. Numer. Anal. 54 (1) (2016) 242–261. doi:http://dx.doi.org/10.1137/15M1014760.

[9] S. Berrone, S. Pieraccini, S. Scialò, Towards effective flow simulations in realistic discrete fracture networks, J. Comput. Phys. 310 (2016) 181–201. doi:http://dx.doi.org/10.1016/j.jcp.2016.01.009.

[10] S. Berrone, S. Pieraccini, S. Scialò, Non-stationary transport phenomena in networks of fractures: Effective simulations and stochastic analysis, Computer Methods in Applied Mechanics and Engineering 315 (2017) 1098 – 1112. doi:http://dx.doi.org/10.1016/j.cma.2016.12.006.

[11] S. Pieraccini, S. Scialò, On a PDE-constrained optimization approach for flow simulations in fractured media, in: Advances in Discretization Methods, Vol. 12 of SEMA SIMAI Springer Series, Springer International Publishing, Switzerland, 2016, pp. 27–45.

[12] J. Warren, P. Root, The behaviour of naturally fractured reservoirs, SPE J. 3 (3) (1963) 245–255.

[13] Z. Chen, G. Huan, Y. Ma, Computational Methods for Multiphase Flows in Porous Media, SIAM, Philadelphia, PA, USA, 2006.

[14] M. Karimi-Fard, L. Durlofsky, K. Aziz, An efficient discrete-fracture model applicable for general-purpose reservoir simulators, SPE J. 9 (2004) 227–236.

[15] T. Sandve, I. Berre, J. Nordbotten, An efficient multi-point flux approximation method for discrete fracturematrix simulations, Journal of Computational Physics 231 (9) (2012) 3784 – 3800. doi:http://dx.doi.org/10.1016/j.jcp.2012.01.023.

[16] C. Alboin, J. Jaffré, J. Roberts, C. Serres, Domain decomposition for flow in porous media with fractures, in: C.-H. Lai, P. E. Bjorstad, M. Cross, O. B. Widlund (Eds.), Proceedings of the 11th International Conference on Domain Decomposition Methods in Greenwich, 1999, pp. 371–379.

[17] P. Angot, F. Boyer, F. Hubert, Asymptotic and numerical modelling of flows in fractured porous media, ESAIM: M2AN 43 (2) (2009) 239–275. doi:10.1051/m2an/2008052.

[18] C. D'Angelo, A. Scotti, A mixed finite element method for Darcy flow in fractured porous media with non-matching grids, ESAIM: M2AN 46 (2) (2012) 465–489. doi:10.1051/m2an/2011148.

[19] R. Ahmed, M. Edwards, S. Lamine, B. Huisman, M. Pal, Control-volume distributed multi-point flux approximation coupled with a lower-dimensional fracture model, Journal of Computational Physics 284 (2015) 462 – 489. doi:http://dx.doi.org/10.1016/j.jcp.2014.12.047.

[20] K. Brenner, M. Groza, C. Guichard, G. Lebeau, R. Masson, Gradient discretization of hybrid dimensional Darcy flows in fractured porous media, Numerische Mathematik 134 (3) (2016) 569–609. doi:10.1007/s00211-015-0782-x.

[21] P. F. Antonietti, L. Formaggia, A. Scotti, M. Verani, N. Verzott, Mimetic finite difference approximation of flows in fractured porous media, ESAIM: M2AN 50 (3) (2016) 809–832. doi:10.1051/m2an/2015087.

[22] K. Brenner, J. Hennicker, R. Masson, P. Samier, Gradient discretization of hybrid-dimensional Darcy flow in fractured porous media with discontinuous pressures at matrix-fracture interfaces, IMA Journal of Numerical Analysis.doi:10.1093/imanum/drw044.

[23] A. Fumagalli, A. Scotti, A numerical method for two-phase flow in fractured porous media with non-matching grids, Advances in Water Resources 62 (2013) 454 – 464. doi:http://dx.doi.org/10.1016/j.advwatres.2013.04.001.

[24] T.-P. Fries, T. Belytschko, The extended/generalized finite element method: an overview of the method and its applications, Internat. J. Numer. Methods Engrg. 84 (3) (2010) 253–304. doi:http://dx.doi.org/10.1002/nme.2914.

[25] H. Huang, T. A. Long, J. Wan, W. P. Brown, On the use of enriched finite element method to model subsurface features in porous media flow problems, Computational Geosciences 15 (4) (2011) 721–736. doi:10.1007/s10596-011-9239-1.

[26] L. Beirão da Veiga, F. Brezzi, A. Cangiani, G. Manzini, L. D. Marini, A. Russo, Basic principles of virtual element methods, Mathematical Models and Methods in Applied Sciences 23 (01) (2013) 199–214.

[27] L. Beirão da Veiga, F. Brezzi, L. D. Marini, Virtual elements for linear elasticity problems, SIAM Journal on Numerical Analysis 51 (2) (2013) 794–812. doi:10.1137/120874746.

[28] B. Ahmad, A. Alsaedi, F. Brezzi, L. D. Marini, A. Russo, Equivalent projectors for virtual element methods, Computers & Mathematics with Applications 66 (2013) 376–391.

[29] F. Brezzi, R. S. Falk, L. D. Marini, Basic principles of mixed virtual element methods, ESAIM: Mathematical Modelling and Numerical Analysis 48 (04) (2014) 1227–1240.

[30] L. Beirão da Veiga, F. Brezzi, L. D. Marini, A. Russo, Virtual element methods for general second order elliptic problems on polygonal meshes, Mathematical Models and Methods in Applied Sciences 26 (04) (2015) 729–750. doi:10.1142/S0218202516500160.

[31] M. Benedetto, S. Berrone, A. Borio, S. Pieraccini, S. Scialò, Order preserving SUPG stabilization for the virtual element formulation of advection-diffusion problems, Comput. Methods Appl. Mech. Engrg. 311 (2016) 18 – 40. doi:10.1016/j.cma.2016.07.043.

[32] M. Benedetto, S. Berrone, S. Scialò, A globally conforming method for solving flow in discrete fracture networks using the virtual element method, Finite Elem. Anal. Des. 109 (2016) 23–36. doi:http://dx.doi.org/10.1016/j.finel.2015.10.003.

[33] M. Benedetto, S. Berrone, A. Borio, S. Pieraccini, S. Scialò, A hybrid mortar virtual element method for discrete fracture network simulations, J. Comput. Phys. 306 (2016) 148–166. doi:http://dx.doi.org/10.1016/j.jcp.2015.11.034.

[34] M. F. Benedetto, S. Berrone, A. Borio, The virtual element method for underground flow simulations in fractured media, in: G. Ventura, E. Benvenuti (Eds.), Advances in Discretization Methods: Discontinuities, Virtual Elements, Fictitious Domain Methods, Springer International Publishing, Cham, 2016, pp. 167–186. doi:10.1007/978-3-319-41246-7_8.

[35] S. Berrone, A. Borio, Orthogonal polynomials in badly shaped polygonal elements for the Virtual Element Method, Finite Elem. Anal. Des. 129 (2017) 14–31. doi:10.1016/j.finel.2017.01.006.

[36] O. Al-Hinai, S. Srinivasan, M. F. Wheeler, Domain decomposition for flow in porous media with fractures, in: SPE Reservoir Simulation Symposium 23-25 February 2013, Houston, Texas, USA, Society of Petroleum Engineers, 2015. doi:10.2118/173319-MS.

[37] L. Formaggia, A. Scotti, F. Sottocasa, Analysis of a Mimetic Finite Difference approximation of flows in fractured media, Technical Report 49/2016, MOX, Mathematical Department, Politecnico di Milano (2016).

[38] L. Beirão da Veiga, K. Lipnikov, G. Manzini, The Mimetic Finite Difference Method for Elliptic Problems, Vol. 11 of Modeling, Simulation & Applications, Springer, 2014.

[39] N. Frih, V. Martin, J. E. Roberts, A. Saâda, Modeling fractures as interfaces with nonmatching grids, Computational Geosciences 16 (4) (2012) 1043–1060. doi:10.1007/s10596-012-9302-6.

[40] I. Aavatsmark, An introduction to multipoint flux approximations for quadrilateral grids, Computational Geosciences 6 (3) (2002) 405–432. doi:10.1023/A:1021291114475.

[41] V. Reichenberger, H. Jakobs, P. Bastian, R. Helmig, A mixed-dimensional finite volume method for two-phase flow in fractured porous media, Advances in Water Resources 29 (7) (2006) 1020 – 1036. doi:http://dx.doi.org/10.1016/j.advwatres.2005.09.001.

[42] H. Hajibeygi, D. Karvounis, P. Jenny, A hierarchical fracture model for the iterative multiscale finite volume method, Journal of Computational Physics 230 (24) (2011) 8729 – 8743. doi:http://dx.doi.org/10.1016/j.jcp.2011.08.021.

[43] N. Makedonska, S. L. Painter, Q. M. Bui, C. W. Gable, S. Karra, Particle tracking approach for transport in three-dimensional discrete fracture networks, Computational Geosciences 19 (5) (2015) 1123–1137. doi:http://dx.doi.org/10.1007/s10596-015-9525-4.

[44] J. D. Hyman, S. Karra, N. Makedonska, C. W. Gable, S. L. Painter, H. S. Viswanathan, dfnworks: A discrete fracture network framework

for modeling subsurface flow and transport, Computers & Geosciences 84 (2015) 10 – 19. doi:http://dx.doi.org/10.1016/j.cageo.2015.08.001.

[45] I. Faille, A. Fumagalli, J. Jaffré, J. E. Roberts, Model reduction and discretization using hybrid finite volumes for flow in porous media containing faults, Computational Geosciences 20 (2) (2016) 317–339. doi:10.1007/s10596-016-9558-3.

[46] R. A. Horn, C. R. Johnson, Matrix Analysis, Cambridge University Press, Cambridge, United Kingdom, 1990.

[47] J. Nocedal, S. J. Wright, Numerical Optimization, Second Edition, Springer, New York, USA, 2006.